Cell Reports

Article

Extracellular vesicle-mediated trafficking of molecular cues during human brain development

Graphical abstract

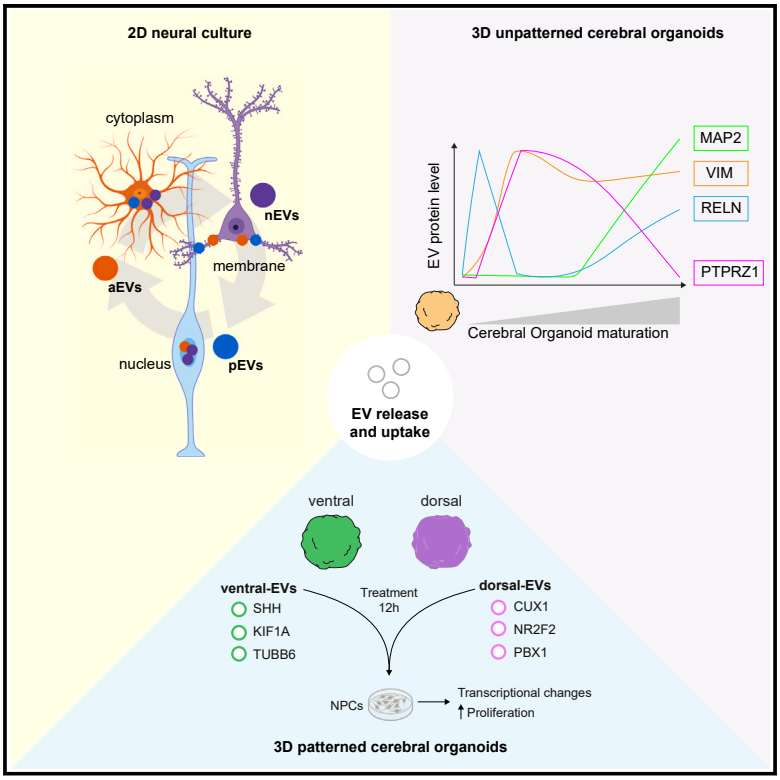

Highlights

- Revealed the proteomic heterogeneity of EVs secreted by neural cells and COs
- Neural cells present different EV uptake mechanisms
- EVs traffic molecular cues relevant in brain development
- EV treatment leads to transcriptional changes and increased proliferation

Authors

Andrea Forero, Fabrizia Pipicelli, Sylvain Moser, ..., Giuseppina Maccarrone, Rossella Di Giaimo, Silvia Cappello

Correspondence

digiaimo@unina.it (R.D.G.), silvia.cappello@bmc.med.lmu.de (S.C.)

In brief

Forero et al. highlight heterogeneity in the protein content of EVs secreted by neural cells and cerebral organoids. Their findings show that neural cells present different EV uptake mechanisms and that EV treatment exerts transcriptional changes and an increase in proliferation in NPCs.

Forero et al., 2024, Cell Reports *43*, 114755
October 22, 2024
https://doi.org/10.1016/j.celrep.2024.114755

CellPress

Cell Reports

CellPress
OPEN ACCESS

Article

Extracellular vesicle-mediated trafficking of molecular cues during human brain development

Andrea Forero,[1,2,11] Fabrizia Pipicelli,[1,3,11] Sylvain Moser,[1,3] Natalia Baumann,[4] Christian Grätz,[5] Mariano Gonzalez Pisfil,[6] Michael W. Pfaffl,[5] Benno Pütz,[1] Pavel Kielkowski,[7] Filippo M. Cernilogar,[8,9] Giuseppina Maccarrone,[1] Rossella Di Giaimo,[1,10,*] and Silvia Cappello[1,2,12,*]

[1]Max Planck Institute of Psychiatry, Munich, Germany
[2]Division of Physiological Genomics, Biomedical Center (BMC), Faculty of Medicine, Ludwig Maximilian University (LMU), Munich, Germany
[3]International Max Planck Research School for Translational Psychiatry, Munich, Germany
[4]Department of Basic Neurosciences, University of Geneva, Geneva, Switzerland
[5]Division of Animal Physiology and Immunology, Technical University of Munich, Freising, Germany
[6]Core Facility Bioimaging and Walter-Brendel-Centre of Experimental Medicine, Biomedical Center, Ludwig Maximilian University, Munich, Germany
[7]Department of Chemistry, Ludwig Maximilian University, Munich, Germany
[8]Division of Molecular Biology, Biomedical Center (BMC), Faculty of Medicine, Ludwig Maximilian University, Munich, Germany
[9]Department of Science and Technological Innovation, University of Piemonte Orientale, Alessandria, Italy
[10]Department of Biology, University of Naples Federico II, Naples, Italy
[11]These authors contributed equally
[12]Lead contact
*Correspondence: digiaimo@unina.it (R.D.G.), silvia.cappello@bmc.med.lmu.de (S.C.)
https://doi.org/10.1016/j.celrep.2024.114755

SUMMARY

Cellular crosstalk is an essential process influenced by numerous factors, including secreted vesicles that transfer nucleic acids, lipids, and proteins between cells. Extracellular vesicles (EVs) have been the center of many studies focusing on neurodegenerative disorders, but whether EVs display cell-type-specific features for cellular crosstalk during neurodevelopment is unknown. Here, using human-induced pluripotent stem cell-derived cerebral organoids, neural progenitors, neurons, and astrocytes, we identify heterogeneity in EV protein content and dynamics in a cell-type-specific and time-dependent manner. Our results support the trafficking of key molecules via EVs in neurodevelopment, such as the transcription factor YAP1, and their localization to differing cell compartments depending on the EV recipient cell type. This study sheds new light on the biology of EVs during human brain development.

INTRODUCTION

The events that organize brain structure during development include neurogenesis, cell migration, and axon projection and guidance.[1–3] In this dynamic context, cell-to-cell communication is an essential process influenced by factors including cell morphology, adhesion molecules, the local extracellular matrix (ECM), and secreted vesicles.[4–6] Extracellular signals are required during development to establish precise cell numbers, unique cell types, and specific cell migration patterns, positions, and functions.[7–10]

Extracellular vesicles (EVs) are small particles in the brain extracellular environment that have gained interest due to their potential in diagnostics and therapeutics in neurodevelopmental disorders.[11] EVs are secreted by all cells and are classified mostly as exosomes and microvesicles based on their size, composition, and origin. While exosomes are generally smaller (30–200 nm) and released by the fusion of multivesicular bodies with the plasma membrane, microvesicles (of much variable size, 100–1000 nm) are directly shed by the outward blebbing of the plasma membrane.[12] Vesicles travel long distances within and outside of cells, thus impacting crosstalk at several levels and sites. Although EVs are key players in extracellular environment composition, few studies have focused on their functional role during brain development. Studies have shown that neural stem cells release Prominin-1 via EVs,[13] while retinal stem cells release EVs containing developmental transcription factors (TFs), microRNA, and membrane proteins that regulate gene expression in developing mouse and human retinal organoids.[14,15] Neurons and astrocytes *in vitro* have also been shown to secrete EVs containing varied cargoes, such as the L1 adhesion molecule and specific subunits of the glutamate receptor.[16,17] EVs also have physiological and pathological functions, for instance, directing neuronal differentiation and regulating synapse formation in healthy neurons,[16,18,19] as well as in neurodevelopmental disorders such as cortical malformations and autism spectrum disorder.[7,20,21] Recent studies support that EVs can act as carriers of ECM components such as Tenascin C[22,23] and, therefore, regulate cell growth, differentiation, and migration by transporting ECM remodeling cargoes like matrix

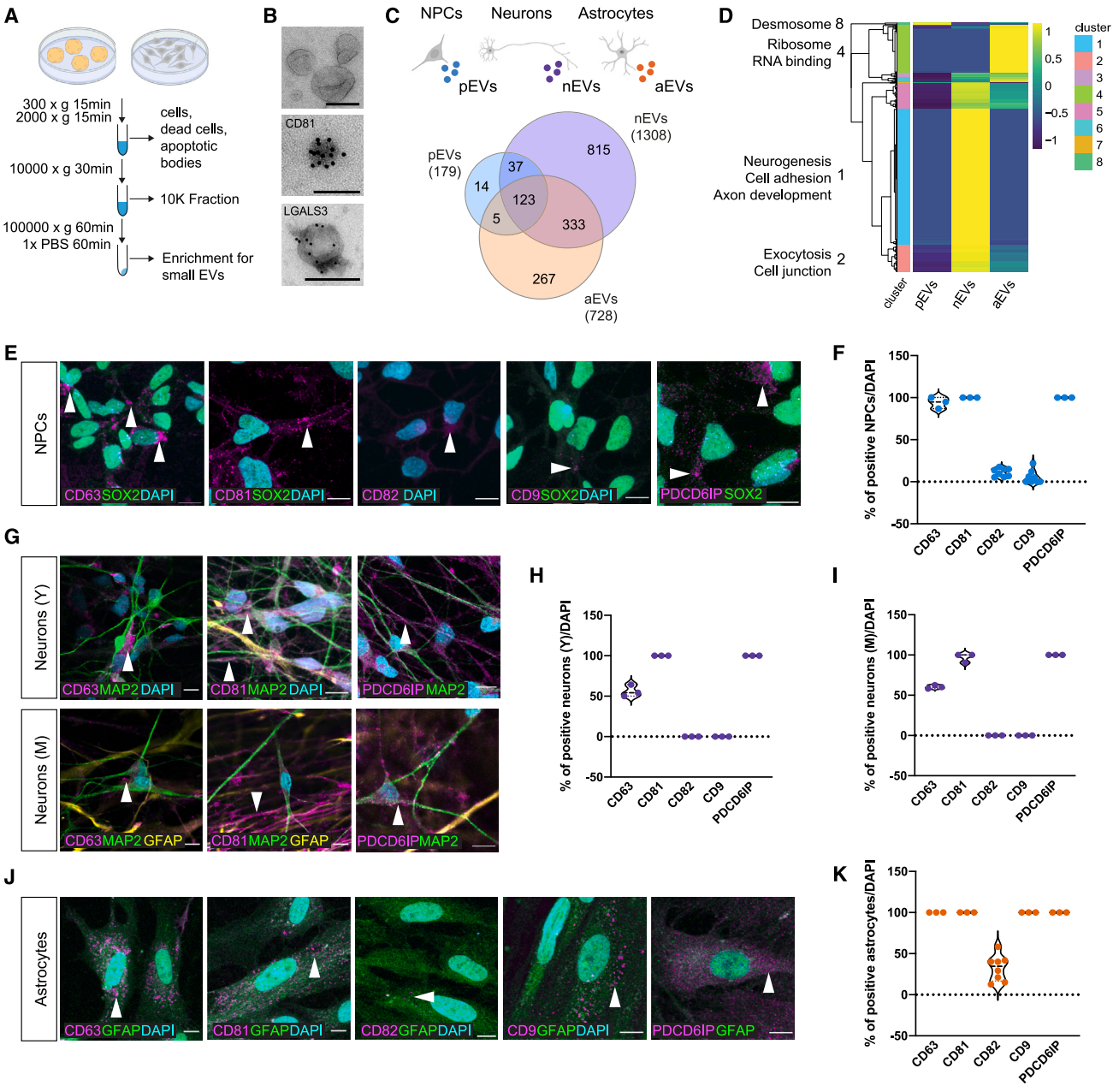

Figure 1. Isolation and cell-type-specific characterization of EVs

(A) Schematic of EV isolation protocol by differential ultracentrifugation. Cell and EVs are generated from control line C1.

(B) Immuno-electron micrographs of CD81 and LGALS3 in EVs collected from CO conditioned media. Scale bar: 100 nm.

(C) Schematic of EVs secreted by 2D cell populations, NPCs (neural progenitor cells; pEVs, blue), neurons (nEVs, purple), and astrocytes (aEVs, orange) (top), and Venn diagram of proteins detected in pEVs, nEVs, and aEVs (bottom).

(D) Heatmap showing hierarchical clusters of proteins detected in pEVs, nEVs, and aEVs. GO enrichments of clusters are displayed. EVs were collected from the conditioned media of 3–5 different wells of cells in culture.

(E) CD63, CD81, CD82, CD9, and PDCD6IP immunostaining in NPCs (SOX2+, green) (arrowheads). DAPI, cyan. Scale bar: 10 μm.

(F) Quantification of $CD63^+$, $CD81^+$, $CD82^+$, $CD9^+$, and $PDCD6IP^+$ NPCs. Violin plots show the median and interquartile range. Every dot refers to a field of view, each from a different differentiation (biological replicates), n = 3–8 per condition.

(G) CD63, CD81, and PDCD6IP immunostaining in young (Y) neurons (MAP2+, green) (top) and mature (M) neurons (MAP2+, green and GFAP+, yellow) (bottom) (arrowheads). DAPI, cyan. Scale bar: 10 μm.

(H) Quantification of $CD63^+$, $CD81^+$, and $PDCD6IP^+$ neurons(Y). Violin plots show the median and interquartile range. Every dot refers to a field of view, each from a different differentiation (biological replicates), n = 3 per condition.

(legend continued on next page)

metalloproteinases that can alter depositions of different collagen types.[24] Moreover, annexin-enriched osteoblast-derived EVs act as an extracellular site of mineral nucleation in developing stem cell cultures.[25] However, most of these studies have focused on EV content at a single time point in a two-dimensional (2D) cell culture environment.

Here, we present insight into EV release, composition, uptake, and function across varying neural cell types and developmental stages. For this purpose, we use two human brain models: human induced pluripotent stem cell (iPSC)-derived neural cells in 2D monolayer cultures and a 3D model of human brain development, namely cerebral organoids (COs).

RESULTS

EV protein content varies among neural cell types

We hypothesized that during brain development, different cell types secrete vesicles enriched with cell-type-specific proteins. To investigate this, we first isolated a mixed population of small EVs (Figure S1A), containing both exosomes and small microvesicles, from the secreted fraction (culture medium) of 2D monolayer cultures enriched in human iPSC-derived neural progenitor cells (NPCs), neurons, and astrocytes. EV isolation was conducted by differential ultracentrifugation,[26,27] and we further characterized EVs by nanoparticle tracking analysis (NTA) and immunoelectron microscopy with transmembrane (CD81) and intraluminal (LGALS3) markers (Figures 1A, 1B, and S1A). We then profiled the protein content of EVs isolated from our 2D neural cultures by mass spectrometry (Figures 1C, 1D, and S1B; Table S1). The results of the protein profiling validated our EV purification protocol, in accordance with the guidelines provided by the International Society for Extracellular Vesicles.[28] Standard positive EV markers (CD63, TSG101, and PDCD6IP) were present in all our samples, while negative markers (CYC1 and GOLGA2) were undetectable (Figure S1C). The relative abundance of EV proteins was confirmed by western blot (WB) on independent samples (Figure S1D).

Our results showed that the three populations of human iPSC-derived neural cells grown in 2D share less than 8% of the total EV proteins (Figure 1C). EVs from NPCs (pEVs) were the least diverse (in total protein number), with less than 1% of the EV proteins being unique for this cell type (Figures 1C and 1D, cluster 8). On the contrary, neurons exhibited the most unique protein content in EVs (nEVs; Figures 1C and 1D, clusters 1 and 2), suggesting that neurons make extensive use of EVs for cellular crosstalk, as previously shown.[29] Among nEV proteins, we identified an enrichment in proteins linked to neurogenesis, cell adhesion, and axon development. The RNA catabolic process and ribonucleoprotein complex (Figure 1D, cluster 4) were enriched in astrocyte EVs (aEVs). We further performed an immunohistochemical analysis of common EV markers, mainly tetraspanins (CD63, CD81, CD82, CD9) and PDCD6IP, in our 2D neural cultures due to their role in EV biogenesis, specifically cargo loading.[30] We observed some markers being ubiquitously expressed (CD63, CD81, and PDCD6IP), while others presented a more restrictive pattern of expression among different cell types. For instance, CD82 and CD9 were the least abundant overall, limited to a small percentage of NPCs and astrocytes, while absent in both young (Y; 4 weeks in culture) and mature (M; 10 weeks in culture) neurons (Figures 1E–1K). These results are congruent with the expression of these common EV markers among diverse cell types as shown by single-cell RNA sequencing (RNA-seq) analysis of COs (Figures S2A and S2B), which identified CD63, CD81, and PDCD6IP as generally expressed proteins and CD82 and CD9 as enriched in subclasses of neural progenitors. Together, our data show that varying combinations of EV markers are present in different neural cell types, suggesting certain cell-type specificity in EV biogenesis. However, this heterogeneity in EV marker expression is not sufficient to provide insight into the differential loading of EV proteins among the cell types here studied. Therefore, our cell-type-specific proteomic analysis highlighted the release of EVs from different neural cell types loaded with common as well as unique proteins, suggesting the heterogeneity of EVs during human brain development.

EV protein content varies through CO developmental stages

We then investigated EV protein composition using a more complex model system, human iPSC-derived COs, which display a temporal progression similar to that observed in the human fetal brain and not present in our 2D model systems. We performed a systematic proteomic analysis of EVs at different developmental stages in COs (days 15–360; Figure 2A). This analysis was conducted on different batches of organoids derived from a single control cell line, C1, since our aim was to observe changes in EV protein composition at different time points and overcome genetic background variability. We detected a total of 3,791 proteins, with substantial heterogeneity (number of detected proteins) at the different time points (Figures 2B and 2C; Table S1; validation by WB in Figure S3A). The unique protein content for each developmental stage was associated with cell cycle and RNA splicing (day 15), intracellular transport and mitochondrial membrane (day 40), ribosome biogenesis and mitochondrion (day 200), and locomotion, secretion, neuron part, and cell motility (day 360) (Figure 2C). 6.8% of EV proteins were shared across all the developmental stages, including those involved in cell junctions and secretory functions (Figures 2B and 2C). The EV protein difference across CO development suggests unique EV signatures and variety. The total number of EV proteins from 3D COs was strongly increased compared to 2D cultures, suggesting a higher variety in the 3D model system (Figure 2D; Table S1). Day 15 COs are mainly composed by neural progenitors (Figure S3D), while neurons start to be detected

(I) Quantification of $CD63^+$, $CD81^+$, and $PDCD6IP^+$ neurons(M). Violin plots show the median and interquartile range. Every dot refers to a field of view, each from a different differentiation (biological replicates), $n = 3$ per condition.

(J) CD63, CD81, CD82, CD9, and PDCD6IP immunostaining in astrocytes (GFAP+, green) (arrowheads). DAPI, cyan. Scale bar: 10 μm.

(K) Quantification of $CD63^+$, $CD81^+$, $CD82^+$, $CD9^+$, and $PDCD6IP^+$ astrocytes. Violin plots show the median and interquartile range. Every dot refers to a field of view, each from a different differentiation (biological replicates), $n = 3–8$ per condition.

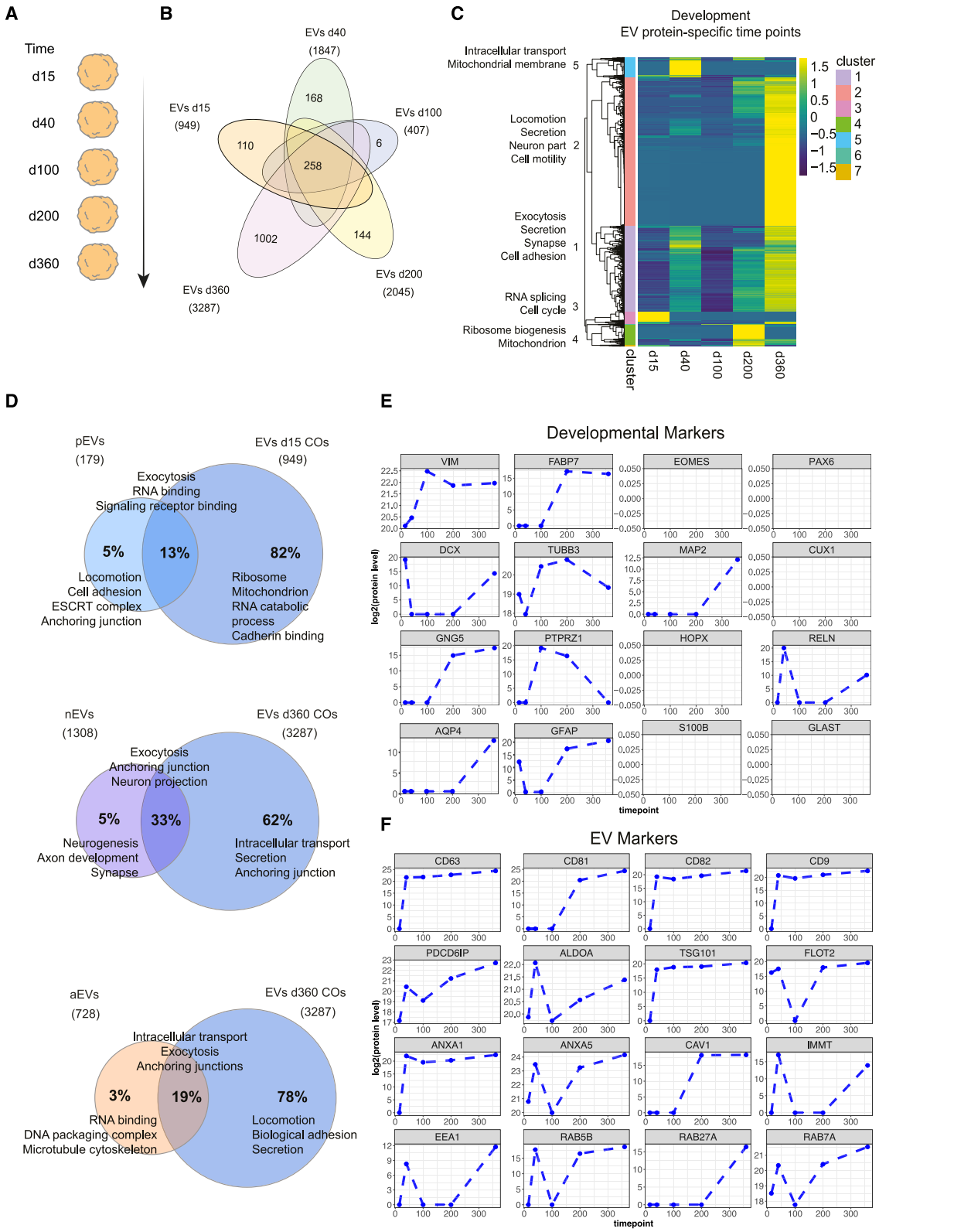

(legend on next page)

only at day 20 (where PAX6 and NESTIN+ progenitor cells are surrounded by very few Doublecortin (DCX)+ neuroblasts; Figure S3E); therefore, we compared pEVs in 2D and 3D day 15 COs. 3D day 360 COs consist of different cell types, including M neurons/astrocytes; therefore, we compared EVs from M astrocytes (aEVs) and M neurons (nEVs) with EVs from day 360 COs. The number of proteins varied greatly, and the enriched Gene Ontology (GO) terms suggest that the 3D environment, composed by a higher heterogeneity of cell types, contributes to EV secretion (Figure 2D). To verify that the shared fraction of proteins between 2D and 3D were not cell-type dependent, we compared the protein content of pEVs and day 15 COs generated from 2 different iPSC lines (Figures 2D and S2C). The results show similar content of shared proteins in the two lines (13% and 17%; Figures 2D and S2C). To assess if the secretion of proteins via EVs followed their physiological pattern of expression in cells, development-associated proteins that were identified in EVs were compared with their cellular gene expression[31] and localization in intracellular vesicles (IVs). Surprisingly, EV proteins did not match gene expression strictly, and their trajectories did not always follow cellular compartmentalization in IVs (Figures 2E, S3B, and S3C), indicating a regulated loading of protein cargo to be released via vesicles. Alternatively, the 3D tissue could interfere with the release of EVs into the medium compared to 2D monolayer cultures. For example, markers for apical radial glia, like VIM and FABP7, already highly expressed early on and throughout development, are secreted in EVs with a comparable dynamic (Figures 2E, S3B, and S3C). Typical markers for basal radial glia, a cell type normally appearing around day 50 in COs, were enriched at different stages in EVs, with PTPRZ1 peaking at day 100 and GNG5 at day 200. Early neuronal markers were detected in EVs, and while DCX peaked at day 15, RELN was strongly enriched at day 40 (Figure 2E). M neuronal markers also exhibited distinctive patterns: TUBB3 was persistently secreted in EVs, while MAP2 was only secreted after 200 days. Glial genes, like AQP4, GFAP, S100B, and GLAST, consistently show an enrichment in the latest stages of CO development, compatible with the process of gliogenesis following neurogenesis. On the contrary, some of the TFs typically expressed in progenitors and neurons during development were not detected in EVs (PAX6, EOMES, HOPX; Figures 2E, S3B, and S3C), suggesting a selective mechanism of protein loading into vesicles. We next examined common EV markers (Figure 2F) and identified unique developmental expression trajectories suggesting EV heterogeneity. Specific microvesicle markers (ANXA1, ANXA5, CAV1, and IMMT) or exosome markers (EEA1, RAB27A, RAB5B, and RAB7A)[32] also displayed a different pattern of secretion during development, suggesting a time- or cell-type-regulated secretion (Figure 2F). Together, our results show a dynamic change in the protein content loading and secretion of EVs depending on the developmental stage and cell type. Moreover, a more complex environment (3D) is associated with increased EV heterogeneity.

EV uptake dynamics is cell-type dependent

Since our proteomic analysis in both 2D neural cultures and 3D COs confirmed heterogeneity in EV protein content, we hypothesized heterogeneity also in the dynamics of EV uptake by receiving cells. To assess this, we collected and fluorescently labeled EVs from our neural cell populations previously described (pEVs, nEVs(Y), nEVs(M), and aEVs; Figures 3A–3C and S4A). Because RFP-labeled NPCs in a microfluidic chamber released RFP+ pEVs that traveled to MAP2+ neurons (Figure S4B), we applied RFP+ or DiI+ EVs directly to our neural cell populations and observed that the uptake mechanism varies between cell types. First, we examined the preferential uptake of each cell type for the different types of EVs by quantifying the percentage of cells positive for donor EVs. NPCs displayed a preference for nEV uptake, both from Y and M neurons, compared to pEVs and aEVs (Figure 3D). Interestingly, while Y neurons uptake both pEVs and aEVs indistinctly, M neurons preferentially uptake EVs released by astrocytes (Figure 3E). Astrocytes appeared to also internalize both pEVs and nEVs, with a higher uptake for M nEVs (Figure 3F). Therefore, EVs generated by the same cell type show a different uptake in recipient cell types. pEVs preferentially target Y neurons, their physiological partners during development (Figure S4C). Similarly, nEVs from Y neurons are internalized mainly by NPCs, while nEVs from M neurons target astrocytes more, a cell type they are more in communication with (Figure S4D). aEV uptake is primarily conducted by neurons (Figure S4E). We also quantified the number of EVs taken up by individual cells (particles per soma) and identified that while most cell types presenting low EV uptake also present low uptake by their individual cells, there are some instances, such as in the uptake of pEVs by NPCs, in which only 26.13% of NPCs uptake pEVs; these cells uptake, on average, 38.90% pEVs per cell compared to 18.70% nEVs (Figures S4F–S4H). We next investigated EV cellular localization following uptake in different cell types using super-resolution microscopy and Imaris 3D rendering (Oxford Instruments). Treatment of NPCs with EVs led to the detection of EVs in their cytoplasm and, more interestingly, their nucleus (Figures 3A and S4I). Both Y and M neurons appeared to internalize EVs in their soma. Additionally, using super-resolution microscopy stimulated emission depletion (STED), we confirmed the docking of EVs along the membrane of neurons at discrete locations, suggesting receptor-mediated signaling

Figure 2. Developmental characterization of EVs

(A) Schematic of analyzed developmental stages in COs. d, day. COs and EVs are generated from control line C1.

(B) Venn diagram of EV proteins at all developmental stages. d, day.

(C) Heatmap showing hierarchical clusters of EV proteins at different time points. GO enrichments of clusters are displayed. EVs were collected from the conditioned media of 15 cm Petri dishes containing 20–30 COs; EVs from different time points were collected from at least 3 different batches of COs.

(D) Venn diagram indicating the percentage of unique and common proteins secreted by NPCs and 15 day COs (top), neurons (8–10 weeks differentiation) and 360 day COs (middle), and astrocytes and 360 day COs (bottom). Functional annotations of GO enrichments of each protein group are shown.

(E) Temporal trajectories of the expression of developmental markers in EVs at different stages.

(F) Temporal trajectories of EV marker expression in EVs at different stages.

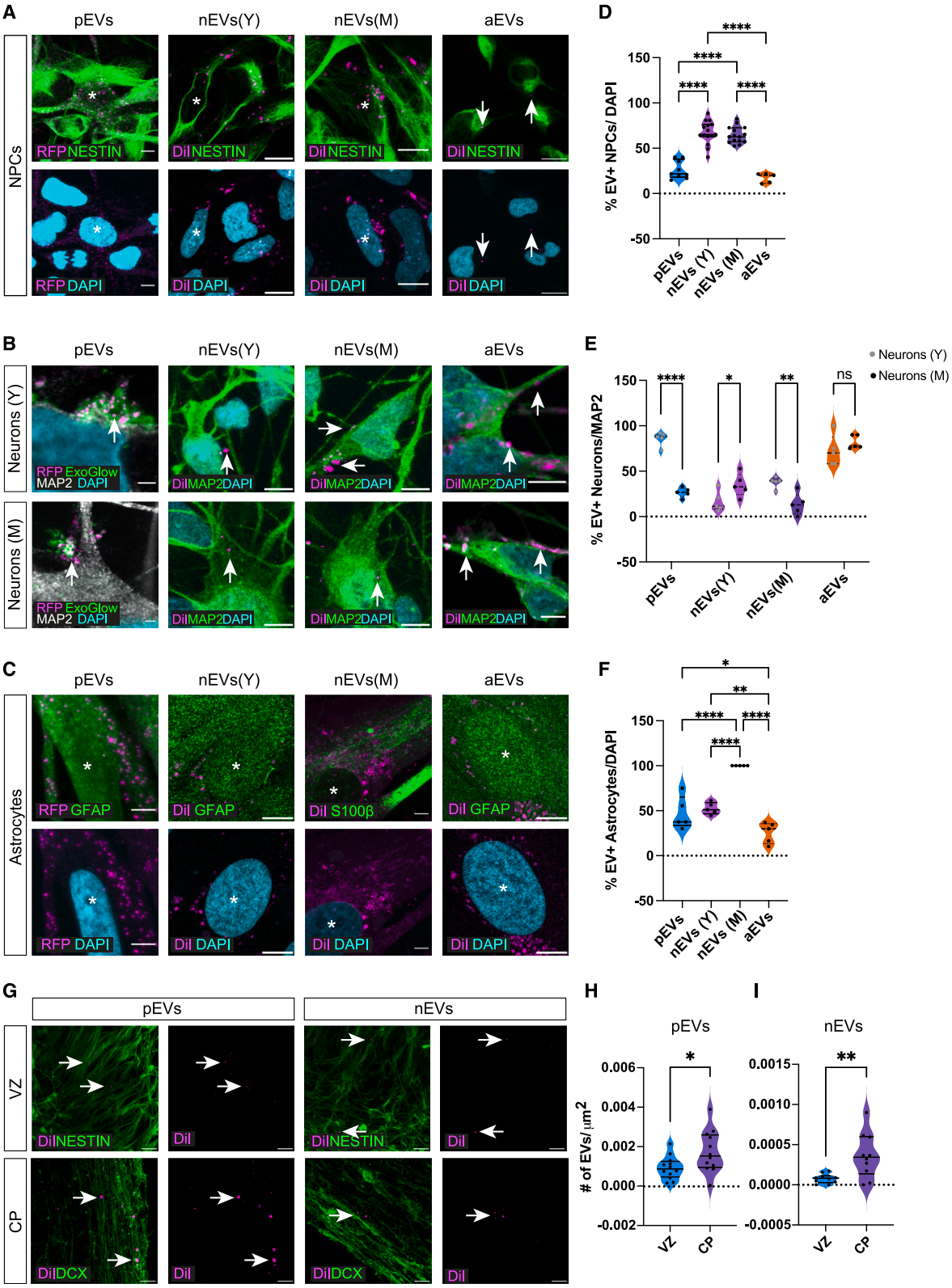

(legend on next page)

(Figures 3B and S4J). Finally, in astrocytes, we detected the uptake of EVs to the cytoplasm; however, these were not transported to the nucleus of the cells as observed in NPCs (Figures 3C and S4K). Alternatively, EVs could fuse by direct contact with the membrane of the receiving cells and induce a cellular response without being phagocytosed.[33]

We then analyzed EV uptake in COs (day 40), focusing on pEVs and nEVs(M) since these COs mainly consist of a ventricular zone (VZ) composed of progenitors and a developing cortical plate (CP) composed of maturing neurons (Figure 3G). Similar to what we observed in the 2D cultures, pEVs are preferentially localized in the CP area compared to VZ progenitors (Figure 3H). nEVs(M) are also localized mainly to the CP; however, their position is more proximal to the VZ and could therefore also be interacting with intermediate progenitors (Figures 3G and 3I).

Together, these data indicate that the mechanism by which EVs interact with recipient cells in both 2D and 3D environments varies, and therefore certain EVs, and naturally their content, could potentially have a higher impact on a specific cell type. In particular, each cell type favors EVs from other cell types compared to self-generated EVs. Moreover, each cell type preferentially takes up EVs secreted by cells that, in physiological conditions, share the same environment. For example, while NPCs mainly take up EVs coming from Y neurons, astrocytes rather favor EVs released by M neurons. Furthermore, the cellular localization of EVs in the recipient cells is distinctly cell-type specific: mostly nuclear in NPCs, membrane bound in neurons, and cytoplasmic in astrocytes, implying that the same EV could have a different signaling mechanism in each target cell.

EVs exert a brain-region-dependent signaling function

Intrigued by the idea that EV content is dependent on cell type and extracellular environment, we investigated whether EVs released from diverse donor cells may have a differential signaling function on recipient cells. For this purpose, we generated ventrally and dorsally patterned forebrain COs (vCOs and dCOs).[34,35] vCOs resemble the ventral telencephalon composed mainly of the ganglionic eminences, which give rise to various types of interneurons, while dCOs resemble the dorsal telencephalon, more specifically, the cerebral cortex. Knowing that 3D organoids are a more suitable model to generate the heterogeneity and diversity of EVs, we used brain-region-specific organoids as different sources of EVs. Thus, we profiled EV proteins from vCOs (vEVs) and dCOs (dEVs) (Figure 4A; Table S1; validation by WB in Figure S5A). vEVs and dEVs shared 62.5% of the total proteins. While vEVs only had a small fraction of unique proteins (2.5%), dEVs contained 35% of unique proteins, showing a greater heterogeneity and suggesting that dorsal and ventral cells make distinct use of EV-mediated communication (Figure 4A). Cell adhesion and motility proteins were enriched in vEVs, while RNA, microRNA (miRNA), and chromatin binding were the main functions for dEV proteins (Figure 4B; Table S1). Among the unique proteins, typical patterning-related proteins were transported either in vEVs (SHH) or dEVs (WNT3A) (Figure 4C). An essential molecular motor (KIF1A) and other proteins associated with neurodevelopmental disorders (RELN) were specific or enriched in vEVs or dEVs (Figure 4C). Single-cell RNA-seq of vCOs and dCOs indicated a similar patterned expression of SHH and KIF1A compared to their EV expression (Figures S5B and S5C). On the contrary, TUBB6 and CHD8 showed a broader RNA expression but a patterned EV protein load (Figures 4C, S5B, and S5C). Interestingly dEVs contained 84 TFs, including TFs fundamental during neurogenesis (examples in Figure 4D; Table S1), while vEVs only contained 50, 48 of which were shared with dEVs. The levels of TFs loaded into EVs did not strictly correspond with their expression levels (Figures S5B and S5C), suggesting a regulated secretion of TFs by specific cell types. To dissect if EVs, and particularly the TFs contained in EVs, have a functional role during cellular crosstalk, we investigated transcriptional changes on cells exposed to EVs. We performed RNA-seq analysis on NPCs acutely treated (12 h) with vEVs and dEVs (Figure 4E). The NPC transcriptome was significantly altered upon EV treatment, particularly upon treatment with dEVs compared to vEVs

Figure 3. EV uptake dynamics in 2D neural cell cultures and 3D COs

Cells and COs are generated from control line C1. EVs are from C1 and an RFP-labeled line (see below).

(A) Immunostaining indicating the uptake of pEVs, nEVs(Y), nEVs(M), and aEVs (magenta) by NPCs (NESTIN+). Asterisks indicate EV receiving cells, and arrows point to EVs detected in cells. DAPI, cyan. Scale bars: full image, 10 μm; close-up, 5 μm.

(B) Immunostaining indicating uptake of pEVs, nEVs(Y), nEVs(M), and aEVs (magenta) by Y (top) and M (bottom) neurons (MAP2+). Arrows point to EVs detected in cells. DAPI, cyan. Scale bars: full image, 10 μm; close-up, 1 μm.

(C) Immunostaining indicating uptake of pEVs, nEVs(Y), nEVs(M), and aEVs (magenta) by astrocytes (GFAP+ or S100b+). Asterisks indicate EV receiving cells. DAPI, cyan. Scale bars: full image, 10 μm; close-up, 5 μm.

(D) Quantification of EV+ NPCs following treatment with pEVs, nEVs(Y), nEVs(M), and aEVs. Data are represented as mean and ±SEM. Every dot refers to a field of view; $n = 9$ (pEVs), $n = 15$ (nEVs(M)), $n = 15$ (nEVs(Y)), and $n = 5$ (aEVs). Statistical significance is based on a one-way analysis of variance (ANOVA); $^{****}p < 0.0001$.

(E) Quantification of EV+ neurons(Y) and neurons(M) following treatment with pEVs, nEVs(Y), nEVs(M), and aEVs. Data are represented as mean and ±SEM. Every dot refers to a field of view; $n = 5$ (pEVs), $n = 5$ (nEVs(M)), $n = 5$ (nEVs(Y)), and $n = 5$ (aEVs). Statistical significance is based on a one-way ANOVA; $^{*}p < 0.05$, $^{**}p < 0.01$, $^{****}p < 0.0001$, and ns, not significant.

(F) Quantification of EV+ astrocytes following treatment with pEVs, nEVs(Y), nEVs(M), and aEVs. Data are represented as mean and ±SEM. Every dot refers to a field of view; $n = 5$ (pEVs), $n = 5$ (nEVs(M)), $n = 5$ (nEVs(Y)), and $n = 5$ (aEVs). Statistical significance is based on a one-way ANOVA; $^{*}p < 0.05$, $^{**}p < 0.01$, and $^{****}p < 0.0001$.

(G) Immunostaining indicating the uptake of pEVs and nEVs(M) (magenta) in the ventricular zone (VZ; NESTIN+) and cortical plate (CP; DCX+) of d40 COs. Arrows point to EVs detected in each region. Scale bar: 100 μm.

(H) Quantification of pEVs detected in the VZ (NESTIN+) and CP (DCX+) of day 40 COs. Data are represented as mean and ±SEM. Every dot refers to a field of view; $n = 12$ per condition. Statistical significance is based on a Student's t test; $^{*}p < 0.05$.

(I) Quantification of nEVs (M) detected in the VZ (NESTIN+) and CP (DCX+) of day 40 COs. Data are represented as mean and ±SEM. Every dot refers to a field of view; $n = 10$ per condition. Statistical significance is based on a Student's t test; $^{**}p < 0.01$.

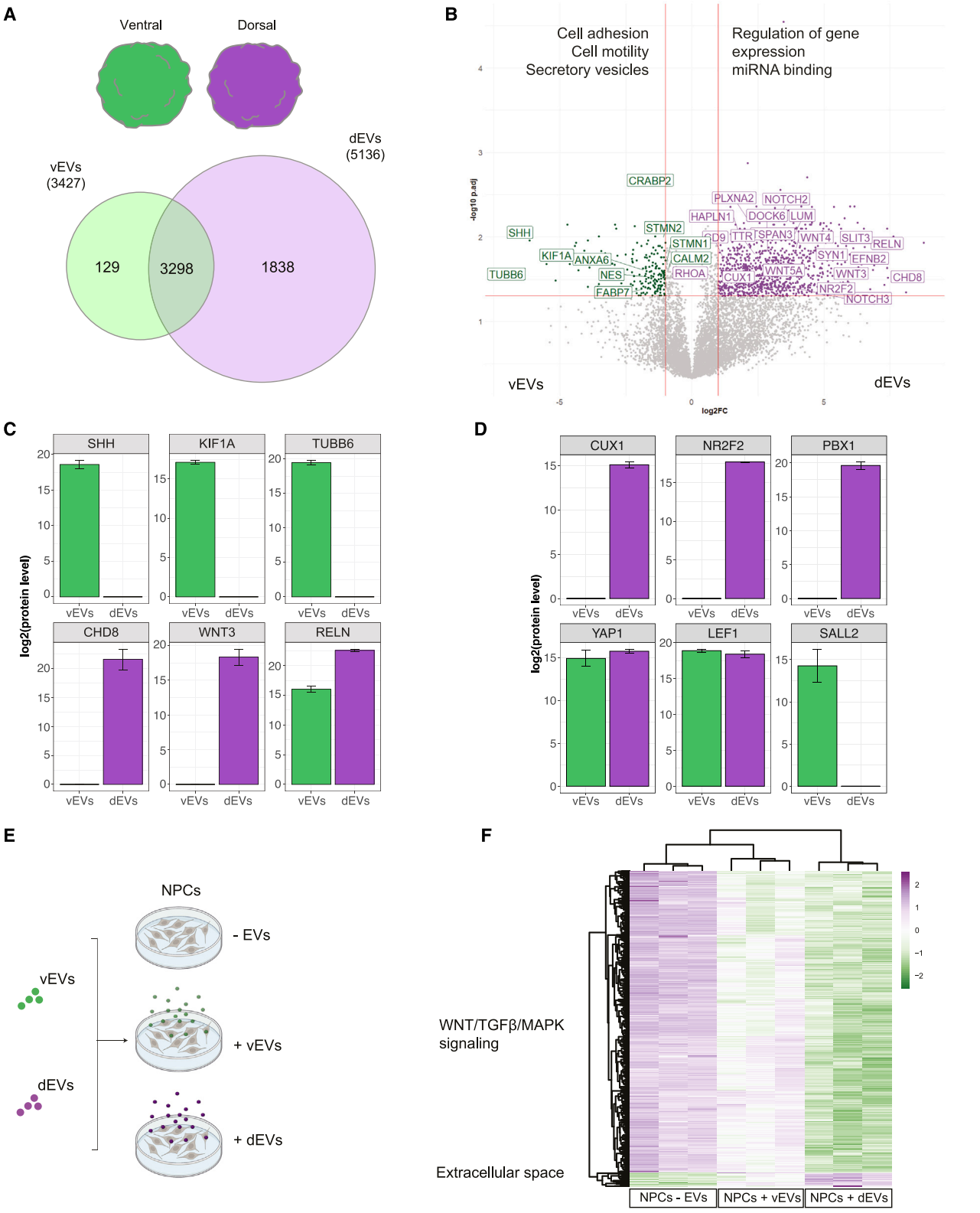

(legend on next page)

(Figure 4F; Table S1). Interestingly, GO terms associated with patterning pathways (e.g., WNT and transforming growth factor β [TGF-β] signaling[36]) were found to be dysregulated in the recipient NPCs. In addition, downstream target genes were differentially expressed according to the type of donor EVs (Figures S5D and S5E). To confirm if these transcriptional changes are due to the differential uptake of vEVs vs. dEVs in NPCs, we conducted an EV uptake assay, which showed no differences in the uptake of these two types of EVs by receiving NPCs (Figure S5D). We can therefore attribute the changes in transcription following differential EV treatment (vEVs vs. dEVs) to the varying content trafficked by each type of EV and not by a difference in their uptake.

Taken together, these results indicated that different cell fate trajectories, for example, excitatory vs. inhibitory, lead to specialized signaling mediated by EVs.

TFs transported via EVs have a signaling function on recipient cells

To identify if some of the transcriptional changes observed in NPCs exposed to EVs were caused by TFs contained in vEVs and dEVs, we analyzed the expression of their targets. BIRC5 (target of YAP1), ECT2 and RACGAP1 (targets of CUX1), and HEY1 and HEY2 (targets of NR2F2) were significantly altered according to the TF enrichment in the patterned EVs (Figures 5A, S5E, and S5F). Since YAP1 is known to be highly expressed in NPCs[37] and is secreted by NPCs via EVs at early stages of human development (Figure 5B), we tested if we could track its journey from secretion to uptake. To achieve this, donor NPCs were first transfected with a FLAG-YAP1 plasmid, then EVs containing FLAG-YAP1 were collected from their medium and used to treat recipient NPCs, which do not express FLAG-YAP1 (Figures 5C and 5F). Immunostaining with FLAG and YAP1 antibodies performed in the recipient NPCs exposed to the FLAG-YAP1 EVs revealed the presence of FLAG in the cytoplasm and nucleus of these cells (Figures 5D and 5E) with a preferential nuclear localization (arrowheads). Increased YAP1 immunofluorescence (IF) intensity was detected in the nucleus (defined by yellow outlines) of receiving cells compared to treatment with control EVs (Figures 5G and 5H). Finally, to evaluate if the higher nuclear levels of YAP1 in recipient cells also led to a physiological response, we assessed proliferation in the recipient cells 72 h following EV treatment (Figure 5I). As expected, we observed an increase in the percentage of KI67+ proliferating cells, providing evidence for a functional role of YAP1 transported via EVs (Figures 5J and 5K). Altogether, these data support not just the trafficking of TFs via EVs but their physiological effect on recipient cells. Nevertheless, we were intrigued by the question of whether the breakdown of the nuclear envelop occurring during mitosis contributed to the transport of EVs into the nuclei of NPCs. We particularly focused on the trafficking of EVs within NPCs, following our observation that this is the only cell type with nuclear uptake of EVs (Figure 3A). To assess this idea, we performed live-cell imaging of NPCs, whose nuclei were labeled with a DNA dye (NucSpot 488) and treated with fluorescently labeled EVs. We imaged cells for 24 h and analyzed them at three stages: pre-mitotic, mitotic, and post-mitotic, based on chromatin condensation (Figure 5L). We observed that out of the 39 mitotic cells identified, 20 of them (51.3%) internalized EVs (EV+ cells) (Figure 5M). At a pre-mitotic stage, 20% of them presented EVs localized within the DNA (Figure 5M). In the post-mitotic daughter cells (DCs), we observe an increase to 80% of the cells with EVs within the nucleus, colocalizing with the DNA staining (Figure 5N). Together, these data suggest that EVs play a role during neurodevelopment, as they contain many regulators, such as TFs, that can be translocated from cell to cell, reach the nucleus, and lead to functional transcriptional changes in receiving cells.

DISCUSSION

In this study, we characterized the developmental-, regional-, and cell-type-specific protein composition of EVs in human neural cells using both a 2D culture system and 3D COs, highlighting the specific function of EVs in physiological conditions. We isolated a mixture of small EVs due to the challenges of isolating specific subtypes of EVs, as exosomes and microvesicles share common markers and sizes.[28] We aimed at identifying cell-type-specific EV markers for NPCs, neurons, and astrocytes, similarly to the work presented in previous studies.[17,38] However, our results emphasize the heterogeneity of EVs and how their composition widely varies through time. EVs collected from COs clearly show that EV protein content does not strictly follow RNA expression, nor protein packaging within IVs, pointing toward a regulated dynamic process in EV protein loading that changes at different developmental stages. This is not surprising, as protein levels do not always reflect RNA expression for different reasons, including protein turnover, stability, degradation, and compartmentalization.[33] Intriguing is the comparison between IVs and EVs, which highlights the heterogeneous intracellular trafficking of vesicles. Therefore, we consider that the EV protein

Figure 4. Brain-region-dependent signaling function of EVs

COs and EVs are generated from control lines C1 and C3.

(A) Schematic of brain-region-specific COs, vCOs (ventral, green) and dCOs (dorsal, purple) (top), and Venn diagram of vCO EV (vEV) and dCO EV (dEV) proteins (bottom).

(B) Volcano plot of protein level of vEVs and dEVs from 40-day-old COs, plotting the negative log10 q-values (false discovery rate [FDR]) of all proteins against their log2 fold change (dEVs vs. vEVs). Significantly expressed proteins ($q < 0.05$) are labeled (vEVs, green; dEVs, purple). GO enrichments are shown. EVs were collected from the conditioned media of 15 cm Petri dishes containing 20–30 COs.

(C) Bar plots showing the expression of brain-region-specific markers in vEVs and dEVs. Data are represented as mean ± SD of technical replicates. $n = 2$ control (CTRL) lines and 2 EPM1 lines.

(D) Bar plots showing the expression of transcriptions factors in vEVs and dEVs. Data are represented as mean ± SD of technical replicates. $n = 2$ CTRL lines and 2 EPM1 lines.

(E) Schematic of acute treatment (12 h) of NPCs with brain-region-specific CO EVs (vEVs, ventral, green; dEVs, dorsal, purple).

(F) Heatmap showing differentially regulated genes in NPCs after treatment with vEVs and dEVs vs. no EV treatment. $n = 3$ replicates per condition.

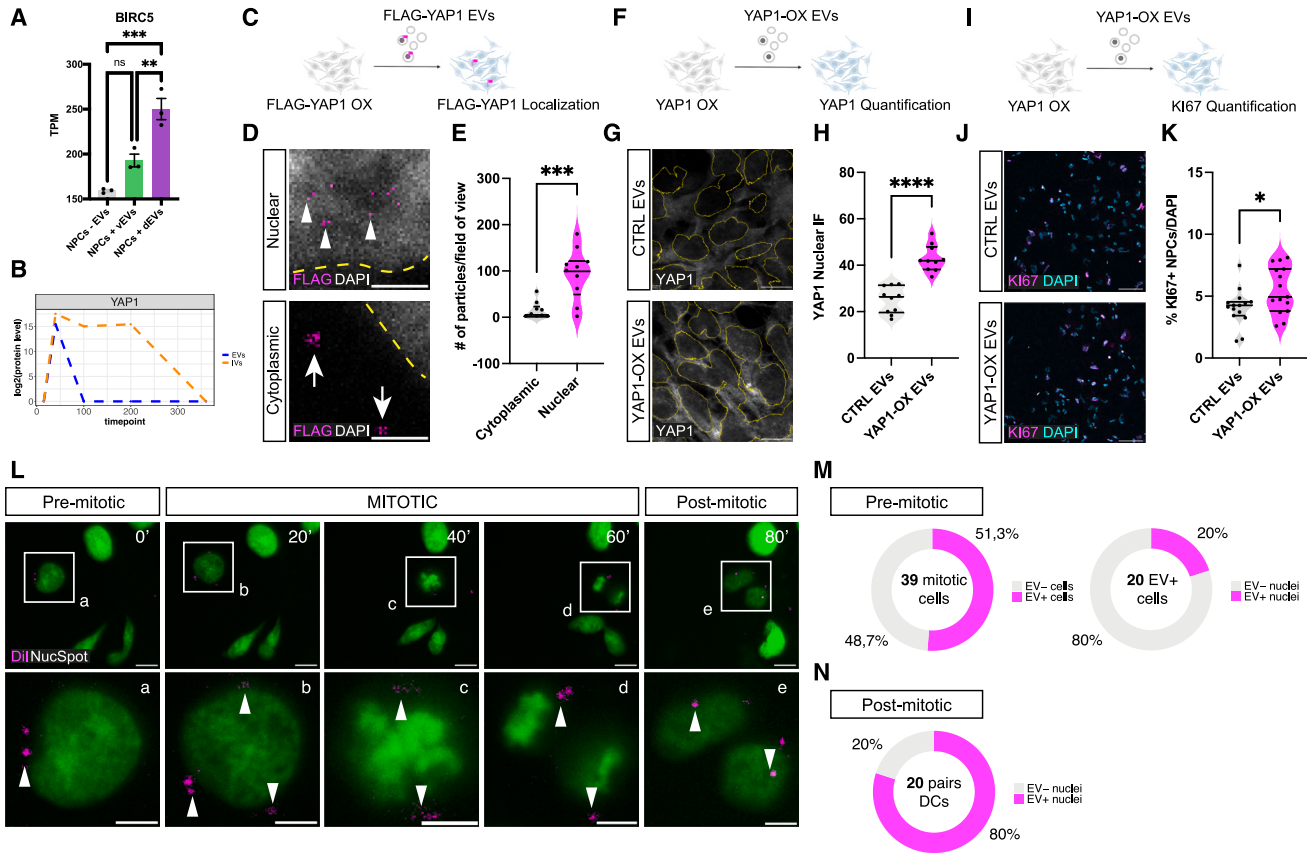

Figure 5. Trafficking of transcription factors via EVs in recipient cells

Cells and EVs are generated from control line C1.

(A) Bar plot showing the expression (TPM [transcripts per million]) of BIRC5 in NPCs after treatment with no EVs, vEVs, and dEVs. Data are represented as mean and ±SEM. $n = 3$ (per condition). Statistical significance is based on a one-way ANOVA; $^{**}p < 0.01$ and $^{***}p < 0.001$.

(B) Temporal trajectory of YAP1 expression in EVs and IVs at different stages of CO development.

(C) Schematic of treatment with FLAG-YAP1 EVs derived from FLAG-YAP1-overexpressing (FLAG-YAP1-OX) NPCs for the localization of FLAG-YAP1 in receiving NPCs.

(D) Immunostaining indicating uptake of FLAG-YAP1 EVs (magenta) by NPCs (nuclear, top; cytoplasmic, bottom) with a yellow outline delimiting the cell nuclei. Arrowheads point to EV localization in the nucleus, and arrows point to EV localization in the cytoplasm. DAPI, gray. Scale bars: 1 μm.

(E) Quantification of the number of particles (FLAG+) detected in NPCs following treatment with FLAG-YAP1 EVs in the nucleus vs. cytoplasm. Data are represented as mean and ±SEM. Every dot refers to a field of view; $n = 10$ (nuclear) and $n = 9$ (cytoplasmic). Statistical significance is based on a Student's t test; $^{***}p < 0.001$.

(F) Schematic of treatment with YAP1-OX EVs derived from YAP1-OX NPCs for the quantification of YAP1 nuclear expression in receiving NPCs.

(G) Immunostaining of YAP1 in NPCs treated with YAP1-OX EVs with a yellow outline delimiting the cell nuclei. DAPI, cyan. Scale bars: 10 μm.

(H) Quantification of nuclear YAP1 fluorescence intensity (FI) detected in NPCs following treatment with YAP1-OX EVs vs. treatment with control EVs. Data are represented as mean and ±SEM. Every dot refers to a field of view; $n = 10$ (per condition). Statistical significance is based on a Student's t test; $^{****}p < 0.0001$.

(I) Schematic of treatment with YAP1-OX EVs derived from YAP1-OX NPCs for the quantification of proliferative marker Ki67 in receiving NPCs.

(J) Immunostaining of KI67 (magenta) in NPCs treated with YAP1-OX EVs. DAPI, cyan. Scale bar: 100 μm.

(K) Quantification of KI67+ NPCs following treatment with YAP1-OX EVs vs. treatment with control EVs. Data are represented as mean and ±SEM. Every dot refers to a field of view; $n = 10$ (per condition). Statistical significance is based on a Student's t test; $^{****}p < 0.0001$.

(L) Time sequence images of EV uptake (DiI, magenta) by NPC nuclei stained with NucSpot (green) in pre-mitotic, mitotic, and post-mitotic stages. Arrowheads point to EV localization. Scale bars: full image, 10 μm; close-up, 5 μm.

(M) Quantification of pre-mitotic EV uptake by NPCs. Left: percentage of mitotic cells (39 cells) that were EV+ or EV−; right: percentage of EV+ mitotic cells (20 cells) that had EV+ nuclei or EV− nuclei.

(N) Quantification of post-mitotic EV uptake by NPCs. Percentage of pairs of daughter cells (DCs) that had EV+ nuclei or EV− nuclei.

composition is highly dependent on the state of the cell and the environment in which it is developing, as shown by the trajectory of developmental markers. Our results present the first evidence that providing a 3D environment during development is critical for building heterogeneous EVs, therefore emphasizing the contribution of tissue complexity to the landscape of EVs in the extracellular space. An increased number of proteins in EVs at late developmental stages could depend on higher cellular heterogeneity, the presence of M and active neurons, or cell death.

Our data indicate that different cell types use specific mechanisms to receive signals from EVs. These differences in composition and uptake may be responsible for a unique cell-specific crosstalk during brain development. Small EVs (exosomes and microvesicles)[39] partially overlap in size and share many extracellular surface markers, making the identification of specific subtypes not trivial.[40] In addition, they can trigger a response based on the different docking mechanisms and localization in the recipient cells.[33] For example, EVs can bind receptors to the surface of the cell, fuse their membrane, and release the content intracellularly or be internalized by different mechanisms (micropinocytosis, phagocytosis, clathrin-mediated endocytosis, lipid rafts, etc.).

While EVs from donor cells were not selectively loaded with classic transmembrane proteins associated with EVs, recipient cells showed preferential affinity with EVs from cells that were developmentally more related (e.g., NPCs and Y neurons or astrocytes and M neurons). Moreover, the cellular localization of EVs in recipient cells (e.g., nuclear in NPCs, cytoplasmic in astrocytes, and plasma membrane in neurons) indicates specific mechanisms of uptake, suggesting that EVs secreted from the same cell type can trigger different responses in different recipient cells. It was recently reported that the cellular response to EVs is highly dependent on the EV dose used during treatment.[41] Since the dosage of our EV treatment was comparable among cells, it would therefore be of relevance to manipulate the EV dosage used during our EV treatment assays to see if this modifies the pattern of uptake so far observed.

Within proteins loaded into EVs, we focus attention on the trafficking of signaling molecules and TFs. Our data show that not all TFs are transported in EVs; however, some that are relevant for human brain development, such as YAP1, are being loaded and trafficked between cells and exert a physiological function on the receiving cells. This is congruent with previous results showing the transfer of TFs in EVs derived from embryonic stem cells,[42] retinal progenitor cells,[14] and disease models of Alzheimer's disease[43] and various cancers.[44,45] However, these results also highlight the specificity of the proteins trafficked by various cell types. For instance, while a study observed the transport of PAX6 and SOX2 in retinal progenitor EVs, we do not detect these TFs in our EV samples.

Additionally, we observed the transport of EVs to the nucleus of recipient NPCs during mitosis and their localization within the nucleus in the descendant DCs. This is a process we identify as being unique for NPCs but that occurs independent of the origin of the EVs, whether they are derived from NPCs, neurons, or astrocytes. Previous studies have shown that EVs can be engulfed in the nucleus of cancer cells by nuclear envelope invaginations.[46,47] Therefore, these data point toward a mechanism within proliferating cells for the transport and incorporation of EVs within the nucleus. A new, interesting avenue would be to decipher which cytoskeletal components are relevant for this mechanism, as it is known that microtubules, actin, and intermediate filaments are the intracellular highways for EV transport.[48,49]

In conclusion, we provide novel insights into a physiological cell non-autonomous mechanism relevant for human brain development. For the first time, we present a detailed analysis supporting that although EVs present protein heterogeneity dependent on cell type and developmental stages, their biogenesis and release is a regulated process that does not strictly correspond with cellular gene expression. We also highlight the transport of physiologically functional molecules, such as TFs. Taken together, our results shed new light on the complexity of cellular crosstalk that plays a critical role in the regulation of neurodevelopmental processes.

Limitations of the study

A notable limitation of our study is the use of COs to model brain development. While COs represent a significant advance in neuroscience research and offer a more realistic model of human brain development compared to conventional cell cultures, they fall short in replicating the intricate complexity and maturity of the human brain. Specifically, COs typically mirror early developmental phases and may lack the extensive structural and functional organization observed in a fully matured brain. It is also noteworthy that COs lack important cues coming from either missing cell types (e.g., microglia) or missing signals (e.g., cerebrospinal fluid and blood vessels). Therefore, experiments carried out with an *in vivo* model system would be important to further validate our results. Additionally, in this study, we have mostly focused on NPCs to demonstrate that EVs have a role in neurogenesis. However, a more complex system containing a more heterogeneous population of cells would be crucial to provide additional evidence of crosstalk between different cell types.

RESOURCE AVAILABILITY

Lead contact

Further information and requests for resources and reagents should be directed to and will be fulfilled by the lead contact, Prof. Dr. Silvia Cappello (silvia.cappello@bmc.med.lmu.de).

Materials availability

This study did not generate new unique reagents.

Data and code availability

- RNA-seq and single-cell RNA-seq data have been deposited at the Gene Expression Omnibus under GEO: GSE197252 and GSE202874, respectively. The mass spectrometry proteomics data have been deposited to the ProteomeXchange Consortium via the PRIDE[50,51] partner repository with the dataset identifier PXD028438.
- This paper does not report original code.
- Any additional information required to reanalyze the data reported in this paper is available from the lead contact upon request.

ACKNOWLEDGMENTS

We thank I. Miinalainen, M. Ködel, C. Cruceanu, C. Turk, S. Zünd, S. Dietzela, and P. Gressens for technical help and critical discussions. We are grateful to all the members of the Cappello, Nguyen, Baulac, Jabaudon, and Baffet labs for the exciting scientific exchange and development of novel ideas over the past few years. This project is supported by ERA-Net E-Rare (HETEROMICS | 01GM1914), the European Union (ERC Consolidator Grant, ExoDevo | 101043959), the Fritz Thyssen Stiftung, the DFG (CA1205/4-1-RU1232/7-1), Italian Ministry of Foreign Affairs and International Cooperation (MAE02035442023-11-16), FRA2022_lineaB_EXOCSTB_Di_Giaimo, and the Munich Cluster for Systems Neurology (SyNergy).

AUTHOR CONTRIBUTIONS

Conceptualization, S.C. and R.D.G.; methodology, R.D.G., F.P., A.F., G.M., P.K., S.M., C.G., M.W.P., and M.G.P.; investigation, S.C., R.D.G., F.P., A.F., N.B., and F.M.C.; visualization, S.C., F.P., A.F., S.M., B.P., and M.G.P.; funding acquisition, S.C.; supervision, S.C., R.D.G., and G.M.; writing – original draft, S.C.; writing – review & editing, S.C., R.D.G., F.P., and A.F.

DECLARATION OF INTERESTS

The authors declare no competing interests.

STAR★METHODS

Detailed methods are provided in the online version of this paper and include the following:

- KEY RESOURCES TABLE
- EXPERIMENTAL MODEL AND STUDY PARTICIPANT DETAILS
  - Cell lines
- METHOD DETAILS
  - IPSC generation and maintenance
  - Generation of RFP-labelled iPSC lines
  - Generation of unpatterned human cerebral organoids
  - Generation of dorsally- and ventrally- patterned human cerebral organoids
  - NPC, neuron and astrocyte cultures
  - FLAG-YAP1 overexpression and EV exchange
  - EV and IV collection and analysis
  - EV uptake assay in 2D cell cultures
  - EV uptake assay in sectioned COs
  - Immunohistochemistry
  - Imaging
  - Microfluidics chamber
  - Proteomic analysis
  - Validation of proteomic results with automated western blot
  - Single-cell RNA-sequencing
  - Bulk-RNA-sequencing
  - RNAseq analysis
- QUANTIFICATION AND STATISTICAL ANALYSIS
  - Quantification of EV markers in cell types
  - Quantification of EV uptake by cell types
  - Quantification of EV uptake by CO sections
  - Proteomic statistical analysis
  - RNAseq statistical analysis
  - Enrichment analysis

SUPPLEMENTAL INFORMATION

Supplemental information can be found online at https://doi.org/10.1016/j.celrep.2024.114755.

Received: November 22, 2023
Revised: July 3, 2024
Accepted: August 29, 2024
Published: September 19, 2024

REFERENCES

1. Taverna, E., Gotz, M., Huttner, W.B., Siripala, A.D., Welch, M.D., Azzarelli, R., Kerloch, T., Pacary, E., Morgan, D.O., Croft, D.R., et al. (2007). The cell biology of neurogenesis: toward an understanding of the development and evolution of the neocortex. Cell *135*, 465–502. https://doi.org/10.1146/annurev-cellbio-101011-155801.
2. Heng, J.I.T., Chariot, A., and Nguyen, L. (2010). Molecular layers underlying cytoskeletal remodelling during cortical development. Trends Neurosci. *33*, 38–47. https://doi.org/10.1016/j.tins.2009.09.003.
3. Rakic, P. (2009). Evolution of the neocortex: a perspective from developmental biology. Nat. Rev. Neurosci. *10*, 724–735. https://doi.org/10.1038/nrn2719.
4. Peruzzotti-Jametti, L., Bernstock, J.D., Willis, C.M., Manferrari, G., Rogall, R., Fernandez-Vizarra, E., Williamson, J.C., Braga, A., van den Bosch, A., Leonardi, T., et al. (2021). Neural stem cells traffic functional mitochondria via extracellular vesicles. PLoS Biol. *19*, e3001166. https://doi.org/10.1371/journal.pbio.3001166.
5. Pellegrini, L., Bonfio, C., Chadwick, J., Begum, F., Skehel, M., and Lancaster, M.A. (2020). Human CNS barrier-forming organoids with cerebrospinal fluid production. Science *369*, eaaz5626. https://doi.org/10.1126/science.aaz5626.
6. Long, K.R., Newland, B., Florio, M., Kalebic, N., Langen, B., Kolterer, A., Wimberger, P., and Huttner, W.B. (2018). Extracellular Matrix Components HAPLN1, Lumican, and Collagen I Cause Hyaluronic Acid-Dependent Folding of the Developing Human Neocortex. Neuron *99*, 702–719.e6. https://doi.org/10.1016/j.neuron.2018.07.013.
7. Sharma, P., Mesci, P., Carromeu, C., McClatchy, D.R., Schiapparelli, L., Yates, J.R., Muotri, A.R., and Cline, H.T. (2019). Exosomes regulate neurogenesis and circuit assembly. Proc. Natl. Acad. Sci. USA *116*, 16086–16094. https://doi.org/10.1073/pnas.1902513116.
8. Long, K.R., and Huttner, W.B. (2019). How the Extracellular Matrix Shapes Neural Development. Preprint at Royal Society Publishing. https://doi.org/10.1098/rsob.180216.
9. Silva, C.G., Peyre, E., and Nguyen, L. (2019). Cell Migration Promotes Dynamic Cellular Interactions to Control Cerebral Cortex Morphogenesis. Preprint at Nature Publishing Group. https://doi.org/10.1038/s41583-019-0148-y.
10. Di Giaimo, R., Penna, E., Pizzella, A., Cirillo, R., Perrone-Capano, C., and Crispino, M. (2020). Cross Talk at the Cytoskeleton–Plasma Membrane Interface: Impact on Neuronal Morphology and Functions. Int. J. Mol. Sci. *21*, 9133. https://doi.org/10.3390/ijms21239133.
11. Gomes, A.R., Sangani, N.B., Fernandes, T.G., Diogo, M.M., Curfs, L.M.G., and Reutelingsperger, C.P. (2020). Extracellular Vesicles in CNS Developmental Disorders. Int. J. Mol. Sci. *21*, 9428. https://doi.org/10.3390/IJMS21249428.
12. Van Niel, G., D'Angelo, G., and Raposo, G. (2018). Shedding Light on the Cell Biology of Extracellular Vesicles. Preprint at Nature Publishing Group. https://doi.org/10.1038/nrm.2017.125.
13. Marzesco, A.M., Janich, P., Wilsch-Bräuninger, M., Dubreuil, V., Langenfeld, K., Corbeil, D., and Huttner, W.B. (2005). Release of extracellular membrane particles carrying the stem cell marker prominin-1 (CD133) from neural progenitors and other epithelial cells. J. Cell Sci. *118*, 2849–2858. https://doi.org/10.1242/JCS.02439.
14. Zhou, J., Benito-Martin, A., Mighty, J., Chang, L., Ghoroghi, S., Wu, H., Wong, M., Guariglia, S., Baranov, P., Young, M., et al. (2018). Retinal progenitor cells release extracellular vesicles containing developmental transcription factors, microRNA and membrane proteins. Sci. Rep. *8*, 2823–2915. https://doi.org/10.1038/s41598-018-20421-1.
15. Zhou, J., Flores-Bellver, M., Pan, J., Benito-Martin, A., Shi, C., Onwumere, O., Mighty, J., Qian, J., Zhong, X., Hogue, T., et al. (2021). Human retinal organoids release extracellular vesicles that regulate gene expression in target human retinal progenitor cells. Sci. Rep. *11*, 21128. https://doi.org/10.1038/s41598-021-00542-w.
16. Fauré, J., Lachenal, G., Court, M., Hirrlinger, J., Chatellard-Causse, C., Blot, B., Grange, J., Schoehn, G., Goldberg, Y., Boyer, V., et al. (2006). Exosomes are released by cultured cortical neurones. Mol. Cell. Neurosci. *31*, 642–648. https://doi.org/10.1016/J.MCN.2005.12.003.
17. Patel, M.R., and Weaver, A.M. (2021). Astrocyte-derived small extracellular vesicles promote synapse formation via fibulin-2-mediated

TGF-β signaling. Cell Rep. *34*, 108829. https://doi.org/10.1016/j.celrep.2021.108829.

18. Schiera, G., Di Liegro, C.M., and Di Liegro, I. (2015). Extracellular Membrane Vesicles as Vehicles for Brain Cell-to-Cell Interactions in Physiological as well as Pathological Conditions. BioMed Res. Int. *2015*, 152926. https://doi.org/10.1155/2015/152926.
19. Takeda, Y.S., and Xu, Q. (2015). Neuronal Differentiation of Human Mesenchymal Stem Cells Using Exosomes Derived from Differentiating Neuronal Cells. PLoS One *10*, e0135111. https://doi.org/10.1371/JOURNAL.PONE.0135111.
20. Kyrousi, C., O'Neill, A.C., Brazovskaja, A., He, Z., Kielkowski, P., Coquand, L., Di Giaimo, R., D' Andrea, P., Belka, A., Forero Echeverry, A., et al. (2021). Extracellular LGALS3BP regulates neural progenitor position and relates to human cortical complexity. Nat. Commun. *12*, 6298. https://doi.org/10.1038/s41467-021-26447-w.
21. Pipicelli, F., Baumann, N., Di Giaimo, R., Forero-Echeverry, A., Kyrousi, C., Bonrath, R., Maccarrone, G., Jabaudon, D., and Cappello, S. (2023). Non-cell-autonomous regulation of interneuron specification mediated by extracellular vesicles. Sci. Adv. *9*, eadd8164. https://doi.org/10.1126/SCIADV.ADD8164.
22. Albacete-Albacete, L., Sánchez-Álvarez, M., and del Pozo, M.A. (2021). Extracellular Vesicles: An Emerging Mechanism Governing the Secretion and Biological Roles of Tenascin-C. Front. Immunol. *12*, 1425. https://doi.org/10.3389/FIMMU.2021.671485/BIBTEX.
23. Rilla, K., Mustonen, A.M., Arasu, U.T., Härkönen, K., Matilainen, J., and Nieminen, P. (2019). Extracellular vesicles are integral and functional components of the extracellular matrix. Matrix Biol. *75–76*, 201–219. https://doi.org/10.1016/J.MATBIO.2017.10.003.
24. Nawaz, M., Shah, N., Zanetti, B.R., Maugeri, M., Silvestre, R.N., Fatima, F., Neder, L., and Valadi, H. (2018). Extracellular Vesicles and Matrix Remodeling Enzymes: The Emerging Roles in Extracellular Matrix Remodeling, Progression of Diseases and Tissue Repair. Cells *7*, 167. https://doi.org/10.3390/CELLS7100167.
25. Davies, O.G., Cox, S.C., Williams, R.L., Tsaroucha, D., Dorrepaal, R.M., Lewis, M.P., and Grover, L.M. (2017). Annexin-enriched osteoblast-derived vesicles act as an extracellular site of mineral nucleation within developing stem cell cultures. Sci. Rep. *7*, 12639. https://doi.org/10.1038/s41598-017-13027-6.
26. Mathieu, M., Martin-Jaular, L., Lavieu, G., and Théry, C. (2019). Specificities of secretion and uptake of exosomes and other extracellular vesicles for cell-to-cell communication. Nat. Cell Biol. *21*, 9–17. https://doi.org/10.1038/s41556-018-0250-9.
27. Théry, C., Amigorena, S., Raposo, G., and Clayton, A. (2006). Isolation and Characterization of Exosomes from Cell Culture Supernatants and Biological Fluids. Curr. Protoc. Cell Biol. *30*, 3.22.1–3.22.29. https://doi.org/10.1002/0471143030.CB0322S30.
28. Théry, C., Witwer, K.W., Aikawa, E., Alcaraz, M.J., Anderson, J.D., Andriantsitohaina, R., Antoniou, A., Arab, T., Archer, F., Atkin-Smith, G.K., et al. (2018). Minimal information for studies of extracellular vesicles 2018 (MISEV2018): a position statement of the International Society for Extracellular Vesicles and update of the MISEV2014 guidelines. J. Extracell. Vesicles *7*, 1535750. https://doi.org/10.1080/20013078.2018.1535750.
29. Men, Y., Yelick, J., Jin, S., Tian, Y., Chiang, M.S.R., Higashimori, H., Brown, E., Jarvis, R., Yang, Y., and Yang, Y. (2019). Exosome reporter mice reveal the involvement of exosomes in mediating neuron to astroglia communication in the CNS. Nat. Commun. *10*, 4136. https://doi.org/10.1038/s41467-019-11534-w.
30. Andreu, Z., and Yáñez-Mó, M. (2014). Tetraspanins in extracellular vesicle formation and function. Front. Immunol. *5*, 442. https://doi.org/10.3389/FIMMU.2014.00442.
31. Cruceanu, C., Dony, L., Krontira, A.C., Fischer, D.S., Roeh, S., Di Giaimo, R., Kyrousi, C., Kaspar, L., Arloth, J., Czamara, D., et al. (2022). Cell-Type-Specific Impact of Glucocorticoid Receptor Activation on the Developing Brain: A Cerebral Organoid Study. Am. J. Psychiatry *179*, 375–387. https://doi.org/10.1176/APPI.AJP.2021.21010095.
32. D'Acunzo, P., Pérez-González, R., Kim, Y., Hargash, T., Miller, C., Alldred, M.J., Erdjument-Bromage, H., Penikalapati, S.C., Pawlik, M., Saito, M., et al. (2021). Mitovesicles are a novel population of extracellular vesicles of mitochondrial origin altered in Down syndrome. Sci. Adv. *7*, eabe5085. https://doi.org/10.1126/SCIADV.ABE5085.
33. van Niel, G., D'Angelo, G., and Raposo, G. (2018). Shedding light on the cell biology of extracellular vesicles. Nat. Rev. Mol. Cell Biol. *19*, 213–228. https://doi.org/10.1038/nrm.2017.125.
34. Lancaster, M.A., and Knoblich, J.A. (2014). Generation of cerebral organoids from human pluripotent stem cells. Nat. Protoc. *9*, 2329–2340. https://doi.org/10.1038/nprot.2014.158.
35. Bagley, J.A., Reumann, D., Bian, S., Lévi-Strauss, J., and Knoblich, J.A. (2017). Fused cerebral organoids model interactions between brain regions. Nat. Methods *7*, 743–751. https://doi.org/10.1038/nmeth.4304.
36. Falk, S., Wurdak, H., Ittner, L.M., Ille, F., Sumara, G., Schmid, M.-T., Draganova, K., Lang, K.S., Paratore, C., Leveen, P., et al. (2008). Brain Area-Specific Effect of TGF-β Signaling on Wnt-Dependent Neural Stem Cell Expansion. Cell Stem Cell *2*, 472–483. https://doi.org/10.1016/j.stem.2008.03.006.
37. Sahu, M.R., and Mondal, A.C. (2021). Neuronal Hippo signaling: From development to diseases. Dev. Neurobiol. *81*, 92–109. https://doi.org/10.1002/DNEU.22796.
38. You, Y., Muraoka, S., Jedrychowski, M.P., Hu, J., McQuade, A.K., Young-Pearse, T., Aslebagh, R., Shaffer, S.A., Gygi, S.P., Blurton-Jones, M., et al. (2022). Human neural cell type-specific extracellular vesicle proteome defines disease-related molecules associated with activated astrocytes in Alzheimer's disease brain. J. Extracell. Vesicles *11*, e12183. https://doi.org/10.1002/JEV2.12183.
39. Nallakumarasamy, A., Jeyaraman, M., Maffulli, N., Jeyaraman, N., Suresh, V., Ravichandran, S., Gupta, M., Potty, A.G., El-Amin, S.F., Khanna, M., and Gupta, A. (2022). Mesenchymal Stromal Cell-Derived Extracellular Vesicles in Wound Healing. Life *12*, 1733. https://doi.org/10.3390/life12111733.
40. Gurung, S., Perocheau, D., Touramanidou, L., and Baruteau, J. (2021). The exosome journey: from biogenesis to uptake and intracellular signalling. Cell Commun. Signal. *19*, 47. https://doi.org/10.1186/s12964-021-00730-1.
41. Hagey, D.W., Ojansivu, M., Bostancioglu, B.R., Saher, O., Bost, J.P., Gustafsson, M.O., Gramignoli, R., Svahn, M., Gupta, D., Stevens, M.M., et al. (2023). The cellular response to extracellular vesicles is dependent on their cell source and dose. Sci. Adv. *9*, eadh1168. https://doi.org/10.1126/SCIADV.ADH1168/SUPPL_FILE/SCIADV.ADH1168_TABLES_S1_TO_S3.ZIP.
42. Ratajczak, J., Miekus, K., Kucia, M., Zhang, J., Reca, R., Dvorak, P., and Ratajczak, M.Z. (2006). Embryonic stem cell-derived microvesicles reprogram hematopoietic progenitors: evidence for horizontal transfer of mRNA and protein delivery. Leukemia *20*, 847–856. https://doi.org/10.1038/sj.leu.2404132.
43. Goetzl, E.J., Boxer, A., Schwartz, J.B., Abner, E.L., Petersen, R.C., Miller, B.L., Carlson, O.D., Mustapic, M., and Kapogiannis, D. (2015). Low neural exosomal levels of cellular survival factors in Alzheimer's disease. Ann. Clin. Transl. Neurol. *2*, 769–773. https://doi.org/10.1002/ACN3.211.
44. Ung, T.H., Madsen, H.J., Hellwinkel, J.E., Lencioni, A.M., and Graner, M.W. (2014). Exosome proteomics reveals transcriptional regulator proteins with potential to mediate downstream pathways. Cancer Sci. *105*, 1384–1392. https://doi.org/10.1111/CAS.12534.
45. Chen, T.Y., Gonzalez-Kozlova, E., Soleymani, T., La Salvia, S., Kyprianou, N., Sahoo, S., Tewari, A.K., Cordon-Cardo, C., Stolovitzky, G., and Dogra, N. (2022). Extracellular vesicles carry distinct proteo-transcriptomic signatures that are different from their cancer cell of origin. iScience *25*, 104414. https://doi.org/10.1016/j.isci.2022.104414.

46. Corbeil, D., Santos, M.F., Karbanová, J., Kurth, T., Rappa, G., and Lorico, A. (2020). Uptake and Fate of Extracellular Membrane Vesicles: Nucleoplasmic Reticulum-Associated Late Endosomes as a New Gate to Intercellular Communication. Cells *9*, 1931. https://doi.org/10.3390/CELLS9091931.

47. Rappa, G., Santos, M.F., Green, T.M., Karbanová, J., Hassler, J., Bai, Y., Barsky, S.H., Corbeil, D., and Lorico, A. (2017). Nuclear transport of cancer extracellular vesicle-derived biomaterials through nuclear envelope invagination-associated late endosomes. Oncotarget *8*, 14443–14461. https://doi.org/10.18632/ONCOTARGET.14804.

48. Kamal, A., and Goldstein, L.S. (2000). Connecting vesicle transport to the cytoskeleton. Curr. Opin. Cell Biol. *12*, 503–508. https://doi.org/10.1016/S0955-0674(00)00123-X.

49. O'Brien, K., Breyne, K., Ughetto, S., Laurent, L.C., and Breakefield, X.O. (2020). RNA delivery by extracellular vesicles in mammalian cells and its applications. Nat. Rev. Mol. Cell Biol. *21*, 585–606. https://doi.org/10.1038/s41580-020-0251-y.

50. Deutsch, E.W., Bandeira, N., Sharma, V., Perez-Riverol, Y., Carver, J.J., Kundu, D.J., García-Seisdedos, D., Jarnuczak, A.F., Hewapathirana, S., Pullman, B.S., et al. (2020). The ProteomeXchange consortium in 2020: enabling "big data" approaches in proteomics. Nucleic Acids Res. *48*, D1145–D1152. https://doi.org/10.1093/nar/gkz984.

51. Perez-Riverol, Y., Csordas, A., Bai, J., Bernal-Llinares, M., Hewapathirana, S., Kundu, D.J., Inuganti, A., Griss, J., Mayer, G., Eisenacher, M., et al. (2019). The PRIDE database and related tools and resources in 2019: improving support for quantification data. Nucleic Acids Res. *47*, D442–D450. https://doi.org/10.1093/nar/gky1106.

52. Rispoli, A., Cipollini, E., Catania, S., Di Giaimo, R., Pulice, G., van Houte, S., Sparla, F., Dal Piaz, F., Roncarati, D., Trost, P., and Melli, M. (2013). Insights in progressive myoclonus epilepsy: HSP70 promotes cystatin B polymerization. Biochim. Biophys. Acta *1834*, 2591–2599. https://doi.org/10.1016/j.bbapap.2013.09.011.

53. Klaus, J., Kanton, S., Kyrousi, C., Ayo-Martin, A.C., Di Giaimo, R., Riesenberg, S., O'Neill, A.C., Camp, J.G., Tocco, C., Santel, M., et al. (2019). Altered neuronal migratory trajectories in human cerebral organoids derived from individuals with neuronal heterotopia. Nat. Med. *25*, 561–568. https://doi.org/10.1038/s41591-019-0371-0.

54. Di Matteo, F., Pipicelli, F., Kyrousi, C., Tovecci, I., Penna, E., Crispino, M., Chambery, A., Russo, R., Ayo-Martin, A.C., Giordano, M., et al. (2020). Cystatin B is essential for proliferation and interneuron migration in individuals with EPM1 epilepsy. EMBO Mol. Med. *12*, e11419.

55. F, C., and J, L. (2012). A method for stable transgenesis of radial glia lineage in rat neocortex by piggyBac mediated transposition. J. Neurosci. Methods *207*, 172–180. https://doi.org/10.1016/J.JNEUMETH.2012.03.016.

56. Lancaster, M.A., Renner, M., Martin, C.A., Wenzel, D., Bicknell, L.S., Hurles, M.E., Homfray, T., Penninger, J.M., Jackson, A.P., and Knoblich, J.A. (2013). Cerebral organoids model human brain development and microcephaly. Nature *501*, 373–379. https://doi.org/10.1038/nature12517.

57. Boyer, L.F., Campbell, B., Larkin, S., Mu, Y., and Gage, F.H. (2012). Dopaminergic differentiation of human pluripotent cells. Curr Protoc Stem Cell Biol *Chapter 1*, Unit1H-6. https://doi.org/10.1002/9780470151808.sc01h06s22.

58. Gunhanlar, N., Shpak, G., van der Kroeg, M., Gouty-Colomer, L.A., Munshi, S.T., Lendemeijer, B., Ghazvini, M., Dupont, C., Hoogendijk, W.J.G., Gribnau, J., et al. (2018). A simplified protocol for differentiation of electrophysiologically mature neuronal networks from human induced pluripotent stem cells. Mol. Psychiatry *23*, 1336–1344. https://doi.org/10.1038/mp.2017.56.

59. Cappello, S., Gray, M.J., Badouel, C., Lange, S., Einsiedler, M., Srour, M., Chitayat, D., Hamdan, F.F., Jenkins, Z.A., Morgan, T., et al. (2013). Mutations in genes encoding the cadherin receptor-ligand pair DCHS1 and FAT4 disrupt cerebral cortical development. Nat. Genet. *45*, 1300–1308.

60. Schneider, C.A., Rasband, W.S., and Eliceiri, K.W. (2012). NIH Image to ImageJ: 25 years of image analysis. Nat. Methods *9*, 671–675. https://doi.org/10.1038/nmeth.2089.

61. Ferrara, E., Cefaliello, C., Eyman, M., De Stefano, R., Giuditta, A., and Crispino, M. (2009). Synaptic mRNAs are modulated by learning. J. Neurosci. Res. *87*, 1960–1968. https://doi.org/10.1002/jnr.22037.

62. Deun, J.V., Roux, Q., Deville, S., Acker, T.V., Rappu, P., Miinalainen, I., Heino, J., Vanhaecke, F., Geest, B.G.D., De Wever, O., et al. (2020). Feasibility of Mechanical Extrusion to Coat Nanoparticles with Extracellular Vesicle Membranes. Cells *9*, 1797–1799. https://doi.org/10.3390/CELLS9081797.

63. Wiśniewski, J.R., Zougman, A., Nagaraj, N., and Mann, M. (2009). Universal sample preparation method for proteome analysis. Nat. Methods *6*, 359–362. https://doi.org/10.1038/nmeth.1322.

64. Tyanova, S., Temu, T., and Cox, J. (2016). The MaxQuant computational platform for mass spectrometry-based shotgun proteomics. Nat. Protoc. *11*, 2301–2319. https://doi.org/10.1038/nprot.2016.136.

65. Prianichnikov, N., Koch, H., Koch, S., Lubeck, M., Heilig, R., Brehmer, S., Fischer, R., and Cox, J. (2020). MaxQuant Software for Ion Mobility Enhanced Shotgun Proteomics. Mol. Cell. Proteomics *19*, 1058–1069. https://doi.org/10.1074/MCP.TIR119.001720.

66. Cernilogar, F.M., Hasenöder, S., Wang, Z., Scheibner, K., Burtscher, I., Sterr, M., Smialowski, P., Groh, S., Evenroed, I.M., Gilfillan, G.D., et al. (2019). Pre-marked chromatin and transcription factor co-binding shape the pioneering activity of Foxa2. Nucleic Acids Res. *47*, 9069–9086. https://doi.org/10.1093/nar/gkz627.

67. Dobin, A., Davis, C.A., Schlesinger, F., Drenkow, J., Zaleski, C., Jha, S., Batut, P., Chaisson, M., and Gingeras, T.R. (2013). STAR: ultrafast universal RNA-seq aligner. Bioinformatics *29*, 15–21. https://doi.org/10.1093/BIOINFORMATICS/BTS635.

68. Love, M.I., Huber, W., and Anders, S. (2014). Moderated estimation of fold change and dispersion for RNA-seq data with DESeq2. Genome Biol. *15*, 550. https://doi.org/10.1186/S13059-014-0550-8.

69. Watanabe K., Taskesen E., van Bochoven A., and Posthuma D. (2017). Functional mapping and annotation of genetic associations with FUMA. Nature Communications 2017 8:1 *8*, 1–11. https://doi.org/10.1038/s41467-017-01261-5.

STAR★METHODS

KEY RESOURCES TABLE

REAGENT or RESOURCE	SOURCE	IDENTIFIER
Antibodies		
Mouse monoclonal Anti-CD63	Santa Cruz	Cat#sc-5275; Lot#I2719; RRID:AB_627877
Mouse monoclonal Anti-CD81	Santa Cruz	Cat#sc-7637; Lot#K0819; RRID:AB_627190
Rabbit polyclonal Anti-KAI 1	Santa Cruz	Cat#sc-1087; Lot#J2814; RRID:AB_2244586
Mouse monoclonal Anti-CD9	Santa Cruz	Cat#sc-59140; Lot#K1220; RRID:AB_1120766
Mouse monoclonal Anti-PDCD6IP (ALIX)	Santa Cruz	Cat#sc-53540; Lot#I1219; RRID:AB_673819
Rabbit polyclonal Anti-SOX2	Abcam	Cat#ab5603; Lot#2682436; RRID:AB_2286686
Chicken polyclonal Anti-MAP2	Abcam	Cat#ab5392; Lot#GR3366474-1; RRID:AB_2138153
Rabbit polyclonal Anti-GFAP	Agilent Dako	Cat#Z0334; Lot#20080613; RRID:AB_10013382
Chicken polyclonal Anti-RFP	Rockland	Cat#600-901-379S; Lot#30253; RRID:AB_10703148
Mouse monoclonal Anti-NESTIN	EMD Millipore	Cat#MAB5326; Lot#3112610; RRID:AB_2251134
Mouse monoclonal Anti-S100β	Sigma	Cat#S2532; Lot#048M4858V; RRID:AB_477499
Guinea pig polyclonal Anti-DCX	EMD Millipore	Cat#AB2253; Lot#3601335; RRID:AB_1586992
Rabbit polyclonal Anti-KI67	Abcam	Cat#AB15580; RRID:AB_443209
Chicken polyclonal Anti-GFP	Rockland	Cat#600-901-215; RRID:AB_1537403;
Mouse monoclonal Anti-RELN	EMD Millipore	Cat#MAB5366 Lot#3601682; RRID:AB_2285132
Mouse monoclonal Anti-LGALS3 (galectin-3)	Santa Cruz	Cat# sc-53127; Lot#K1918; RRID:AB_629514
Mouse monoclonal Anti-ANXA5 (Annexin V)	Santa Cruz	Cat#sc-74438; Lot#I2717; RRID:AB_1118989
Mouse monoclonal Anti-β-Tubulin III	Sigma	Cat# T8660; Lot#097M4835V; RRID:AB_477590
Rabbit polyclonal Anti-FABP7 (BLBP)	EMD Millipore	Cat#ABN14; Lot#3160120; RRID:AB_10000325
Mouse monoclonal Anti-MEIS1/2/3	Santa Cruz	Cat#sc-101850; Lot#H0817; RRID:AB_2143143
Alexa Fluor® 488 Goat Anti-Chicken IgY (H + L)	ThermoFisher Scientific	Cat#A-11039; RRID:AB_2534096
Alexa Fluor® 647 Goat Anti-Guinea Pig IgG (H + L), highly cross-adsorbed	ThermoFisher Scientific	Cat#A-21450; RRID:AB_2535867
Alexa Fluor® 488 Goat Anti-Mouse IgG (H + L) highly cross-adsorbed	ThermoFisher Scientific	Cat#A-21141; RRID:AB_2535778
Alexa Fluor® 546 Goat Anti-Rabbit IgG (H + L), highly cross-adsorbed	ThermoFisher Scientific	Cat#A-11035; RRID:AB_2534093
Alexa Fluor® 647 Goat Anti-Mouse IgG (H + L) cross-adsorbed	ThermoFisher Scientific	Cat#A-21235; RRID:AB_2535804
Chemicals, peptides, and recombinant proteins		
Vybrant™ Multicolor Cell-Labeling Kit	ThermoFisher Scientific	Cat#V22889
NucSpot® Live Cell Nuclear Stains	Biotium	Cat#40081
Smoothened Agonist (SAG)	EMD Millipore	Cat#566660
IWP-2	Sigma-Aldrich	Cat# I0536

(*Continued on next page*)

Continued		
REAGENT or RESOURCE	SOURCE	IDENTIFIER
Cyclopamine A	Calbiochem	Cat#239803
Critical commercial assays		
miRCURY Exosome Cell/Urine/CSF Kit	Qiagen	Cat#76743
Lipofectamine™ 3000 Transfection Reagent	ThermoFisher Scientific	Cat#L3000015
Chromium Next GEM Chip G Single Cell Kit	10XGenomics	Cat#PN-1000127
Chromium Next GEM Single Cell 3' GEM, Library & Gel Bead Kit v3.1	10XGenomics	Cat#PN-1000128
Single Index Kit T Set A	10XGenomics	Cat#PN-1000213
SMART-Seq v4 Ultra Low Input RNA Kit	Clontech	Cat#634888
Deposited data		
Mass spectrometry proteomics data	ProteomeXchange Consortium	PXD038760
Single-cell RNA-seq dataset	Gene Expression Omnibus	GSE202874
Bulk RNA-seq dataset	Gene Expression Omnibus	GSE197252
Experimental models: cell lines		
BJ (human newborn foreskin fibroblasts)	ATCC	CRL-2522
C3 Control IPSCs	Prof. Dr. Silvia Cappello	N/A
Recombinant DNA		
pCMV-flag YAP2 5SA	Kunliang Guan	Addgene #27371
pEGFP-C1	Rispoli et al.[52]	N/A
PBCAG-eGFP	Joseph Loturco	Addgene #40973
PBCAG-mRFP	Joseph Loturco	Addgene #40996
Software and algorithms		
ImageJ software	NIH	https://imagej.nih.gov/ij/
Imaris (v9.7.2)	Oxford Instruments	https://imaris.oxinst.com/
MaxQuant computational platform (v1.6.17.0)	Max-Planck-Institute of Biochemistry	https://www.maxquant.org/
R v4.1.0	R Core Team	https://www.r-project.org/
R package DEP (v1.15.0)	Arne Smits, Wolfgang Huber	https://www.bioconductor.org/packages/release/bioc/html/DEP.html
R package Seurat (v3.2)	Satija Lab	https://satijalab.org/seurat/
R package pheatmap (v1.0.12)	Raivo Kolde	https://cran.r-project.org/web/packages/pheatmap/index.html
STAR (v2.6.1d)	Alexander Dobin	https://github.com/alexdobin/STAR
R package DESeq2 (v1.32.0)	Michael Love	https://bioconductor.org/packages/release/bioc/html/DESeq2.html
GraphPad Prism 8	GraphPad, Inc	https://www.graphpad.com/scientific-software/prism/
GENE2FUNC software	Posthuma Lab	https://fuma.ctglab.nl/
Other		
900 μm microgroove barrier microfluidics silicone device	Xona Microfluidics	Cat#SND900

EXPERIMENTAL MODEL AND STUDY PARTICIPANT DETAILS

Cell lines

Control iPSC (C1,[53] male; C3,[54] female) and RFP-labelled control IPSC lines were cultured on Matrigel (Corning/VWR International, 354234) coated plates (Thermo Fisher, Waltham, MA, USA) in mTeSR1 basic medium supplemented with 1x mTeSR1 supplement (Stem Cell Technologies, Vancouver, Canada, 85850) at 37°C, 5% CO_2 and ambient oxygen level. Passaging was done using Accutase solution (Sigma Aldrich, St. Louis, MO, USA, A6964) treatment.

METHOD DETAILS

IPSC generation and maintenance

iPSCs were previously reprogrammed from 1 control line of fibroblasts, line C1[53] and, 1 control line of PBMCs, line C3.[54] For control line C1, fibroblasts were obtained from human newborn foreskin biopsies. On Day 1, fibroblast cultures with 70–80% confluency were dissociated using 0.25% trypsin-EDTA (25200056, Life Technologies), counted and seeded on 2.5 × 10–5 NuFF3-RQ human newborn foreskin feeder fibroblasts (GSC-3404, GlobalStem) at two different densities: 2 × 10–4 cells/well and 4 × 10–4 cells/well. Day 2, medium was changed to Pluriton Reprogramming Medium (00–0070, Stemgent) supplemented with 500 ng/mL carrier-free B18R Recombinant Protein (03–0017, Stemgent). Days 3–18, modified mRNA (mmRNA) cocktail was transfected daily combining OCT4, SOX2, KLF4, LIN28 and C-MYC mmRNAs at a 3:1:1:1:1 stoichiometric ratio and Opti-MEM I Reduced Serum Medium (13778150, Thermo Fisher Scientific) in a total volume of 105 μL with a mix of 92 μL Opti-MEM I Reduced Serum Medium and 13 μL Lipofectamine RNAiMAX Transfection Reagent (31985062, Thermo Fisher Scientific) after incubation at room temperature (RT) for 15 min. Cells were transfected for 4 h, then washed, and fresh reprogramming medium supplemented with B18R was added to the cultures. The mmRNA factors were provided by the RNA CORE of the Houston Methodist Hospital and contained the following modifications: 5-methyl CTP, Pseudo-UTP, ARCA cap and a 150-nucleotide poly-A tail. For control line C3, PBMCs were isolated from human blood from a control 39-year-old woman. On the first day, a minimum number of 5 × 10^6 PBMCs were cultured in a 25-cm^2 flask containing 5 mL Erythroid Expansion Medium (IMDM 49% v/v; Ham's F-12 49% v/v; ITS-X 1% v/v; lipid concentrate 1% v/v; l-Glutamine 1% v/v; l-Ascorbic acid 0.005% w/v; BSA 0.5% w/v; 1-thioglycerol 0.0018% v/v; human stem cell factor (SCF) 100 ng/mL; human IL-3 10 ng/mL; IGF-1 40 ng/mL; Erythropoietin (EPO) 2 units/mL, KMS (Janssen-Cilag); holo-transferrin 0.1 mg/mL; Dexamethasone 1 μM). On the following day, cell suspension was transferred into a new 25-cm^2 flask. On days 2, 4, and 6, cells were transferred into a 15-mL conical tube and centrifuged at 300 × *g* for 5 min. Supernatant was removed, and cells were resuspended in 1 mL fresh Erythroid Expansion Medium and plated in a new 25-cm^2 flask containing 5 mL fresh Erythroid Expansion Medium. Transfection was carried out on day 8: Cells were collected in a 15-mL conical tube, centrifuged at 300 × *g* for 5 min and the cell pellet resuspended in 2 mL fresh Erythroid Expansion Medium. The cell number was determined using the LUNA-II Automated Cell Counter from Logos Biosystems according to the manufacturer's instructions. For each nucleofection, 2 × 10^6 culture-expanded erythroid cells were transferred into a 15-mL conical tube and centrifuged at 300 × *g* for 5 min, the supernatant was carefully removed and cells were resuspended in 100 μL $CD34^+$ Cell Nucleofector Solution (Lonza, VAPA-1003). 4 μg MOS (Addgene, 64120), 4 μg MMK (Addgene, 64121), and 2 μg GBX (Addgene, 64123) were added to the cell suspension and mixed well. Cells were electroporated with the reprogramming vectors using the Lonza Nucleofector 2b and program T-016. The electroporated cells were transferred into 2 mL fresh Erythroid Expansion Medium and plated in one well of a 12-well plate and incubated for 2 days at 37°C and 5% CO_2. On day 10, electroporated cells were collected into a 15-mL conical tube and centrifuged at 200 × *g* for 5 min. The cell pellet was resuspended in 1 mL DMEM (Life Technologies, 41965039) supplemented with 10% FCS (Life Technologies, 10270–106) and transferred to one well of a 12-well plate, coated with vitronectin (Life Technologies, A14700). The sealed plate was centrifuged at 200 × *g* for 30 min at 25°C and incubated at 37°C, 5% CO_2. The following day, the medium was carefully removed from the culture and collected in a 15-mL conical tube, and 0.5 mL E8 medium (Life Technologies, A1517001) supplemented with 0.25 mM n-Butyric Acid Sodium Salt (NaB) (Sigma, B-5887; MW 110.1) were added to each well. The tubes were centrifuged at 300 × *g* for 5 min, the supernatant was carefully removed and the cell pellet was resuspended in 0.5 mL E8 medium supplemented with 0.25 mM NaB and plated back to the same well so that there was 1 mL of E8 medium supplemented with 0.25 mM NaB per well. The medium was replaced with fresh E8 medium supplemented with 0.25 mM NaB and changed every second day until large colonies of iPSCs become visible. The absence of genomic rearrangements (>0.2 Mb) of the iPSCs reprogrammed from PBMCs was confirmed by Copy Number Variation analysis (Danecek et al., 2016) performed on genotype data obtained by genome-wide SNP array (Infinium Global Screening Array-24 v1.0; Illumina). Both IPSC lines were then cultured on Matrigel (Corning/VWR International, 354234) coated plates (Thermo Fisher, Waltham, MA, USA) in mTeSR1 basic medium supplemented with 1x mTeSR1 supplement (Stem Cell Technologies, Vancouver, Canada) at 37°C, 5% CO2 and ambient oxygen level. Passaging was done using Accutase solution (Sigma Aldrich, St. Louis, MO, USA, A6964) treatment.

Generation of RFP-labelled iPSC lines

RFP-labelled iPSC lines were generated by transfection iPSC control lines with piggyBac transposase (1 μg) and PB-RFP (1 μg) nucleofection.[55] Single cells of iPSCs were transfected with the Amaxa Nucleofector 2b (program B-016). RFP-positive colonies were picked and cultured on Matrigel (Corning/VWR International, 354234) coated plates in mTeSR1 basic medium (Stem Cell Technologies, 85850) supplemented with 1× mTeSR1 supplement (Stem Cell Technologies, 85850) at 37°C and 5% CO2.

Generation of unpatterned human cerebral organoids

Reprogrammed iPSCs, line C1[53] and line C3,[54] were used to generate human cerebral organoids (hCOs).[34,56] On day 1, iPSCs grown to 70–80% confluency were dissociated using Accutase solution (Sigma Aldrich, St. Louis, MO, USA, A6964) treatment, counted and plated in a 96-well U-bottom plate at a density of 9,000 live cells per 150 μL in low-bFGF hESC medium with ROCK inhibitor (1:100, final concentration 50 μM) to form Embryoid Bodies (EBs). On day 4–5, EBs were transferred to neural induction medium (DMEM-F12 with 1% (v/v) N2 supplement, 1% (v/v) GlutaMAX supplement and 1% (v/v) MEM-NEAA, heparin (final concentration of 1 μg mL^{-1})) to

promote the induction of primitive neuroepithelia. 4–5 days later, EBs were embedded in Matrigel (Corning/VWR International, 354234) droplets and kept in static culture in differentiation medium without vitamin A containing 1:1 mixture of DMEM/F12 and Neurobasal supplemented with 1:200 N2 supplement (Invitrogen), 1:100 B27 supplement without vitamin A (Invitrogen), 3.5 mL L21 2-mercaptoethanol, 1:4,000 insulin (Sigma), 1:100 Glutamax (Invitrogen), 1:200 MEM-NEAA. 4–5 days following the embedding, organoids were transferred to an orbital shaker in differentiation medium as above, except B27 supplement with vitamin A (Invitrogen) was used. Organoids were kept in 10-cm dishes on a shaker at 37°C, 5% CO2 and ambient oxygen level with medium changes every 3–4 days.

Generation of dorsally- and ventrally- patterned human cerebral organoids

Patterned human cerebral organoids (dorsal and ventral) were generated as previously described.[51] Briefly, embryoid bodies (EBs) were guided to generate ventral and dorsal identities. iPSCs were dissociating into single cells using Accutase (Sigma-Aldrich, A6964), and approximately 9000 cells were transferred to one well of an ultralow-attachment 96-well plate (Corning). Five days later, during the neuronal induction, EBs were treated individually with Smoothened Agonist (SAG) (1:10,000) (Millipore, 566660) and IWP-2 (1:2000) (Sigma-Aldrich, I0536) to promote a ventral identity and with cyclopamine A (1:500) (Calbiochem, 239803) for a dorsal identity. Following 7 days, EBs were embedded in a Matrigel (Corning/VWR International, 354234) droplet. After this point, the patterned organoids were cultured following the same guidelines used for unpatterned organoids (see generation of unpatterned human cerebral organoids).

NPC, neuron and astrocyte cultures

Neural progenitor cells (NPCs) were generated by following Basic Protocol 1,[57] with the exception that FGF8 and SHH were replaced by FGF2 (Peprotech, 100-18b-50) in the neural progenitor medium (NPM). Briefly, iPSCs were cultured in 10 cm plates in neural induction medium (NIM; DMEM/F12 medium base, 1X N2-supplement (100X), 1X B-27 supplement (50X)), for approximately two days, until large, nearly touching colonies developed. Colonies were then detached using collagenase solution (….) and seeded in an ultra-low-attachment plate for the generation of EBs. After 1 week, EBs were transferred to a 10 cm polyornithine/laminin-coated plate in NIM, and 1 week later, EBs containing neural rosettes were manually picked using a 200 μL (P200) pipet tip. These clumps were then cultures in a new polyornithine/laminin-coated plate in NPM (DMEM/F12 medium base, 1X N2-supplement (100X), 1X B-27 supplement (50X), FGF2 (20 ng/mL) and passaged 1:3 weekly for up to 15 passages. NPCs were generated from three control iPSC lines, line C1,[53] line C3,[54] and one RFP-labelled line[21] (see "IPSCs culture" and "Generation of labeled iPSC lines"), which generated a ratio of 60% neurons and 40% astrocytes in accordance with this protocol, providing electrophysiologically mature neurons in a more physiological environment. Neural differentiation was conducted as previously described,[58] which generates a mixture of neuronal types. In summary, 20,000 cells/well were seeded in 24-well plates coated with polyornithine/laminin in neural differentiation media (Neurobasal as medium base, 1X N2-supplement (100X), 1X B-27 supplement (50X)). Astrocytes were isolated from 8-month-old organoids as follows: Organoids were transferred to a 15 mL falcon tube and washed 1 time with 1xPBS. For dissociation, they were placed in Accutase solution (A6964, Sigma Aldrich, St. Louis, MO, USA) pipetted up and down 5–10 times with a P1000 tip, and then placed in the incubator for 10 min at 37°C, followed by 5 times pipetting for a second time. The dissociated cells were then centrifuged at 300 x g for 3 min and resuspended in *NDM+A media* (DMEME/F12+Glutamax and Neurobasal medium in a ratio 1:1 supplemented with 1:100 N2-supplement (100X), 1:100 B-27 supplement (50X), 0.5% of MEM Non-Essential Amino Acids Solution (100X), 0.5% GlutaMAX Supplement, 50 μM of 2-mercaptoethanol (50 mM), antibiotic antimycotic Solution (100×) and Insulin 2.5 μg/mL) for 24 h. The next day, the cells were transferred to Matrigel Basement Membrane Matrix LDEV-free (Corning, 354234) coated plates. One day later the media was changed to Astrocyte media (89% DMEM/F12+Glutamax, 10% fetal bovine serum, 1% Antibiotic-Antimycotic). The astrocytes obtained were characterized by immunostaining and were positive for astrocytic markers such as SOX9, s100B, NFIA, and negative for neuronal markers MAP2 and NeuN. All the cells were kept in an incubator at 37°C, 5% CO2 and ambient oxygen level with medium changes every 2–3 days.

FLAG-YAP1 overexpression and EV exchange

NPCs were transfected with an FLAG-YAP1 plasmid (Addgene #27371,[59]) and a control plasmid (pEGFP-C1 plasmid) using the Lipofectamine 3000 Transfection Reagent (ThermoFisher Scientific, USA) as instructed in the protocol. 72h following the transfection, the conditioned media from the NPCs was collected for EV collection (see EV collection and analysis). The collected EVs carrying FLAG-YAP1 were then added to a new set of NPCs. The cells were prepared for immunofluorescence after 18h of the treatment and imaged using confocal microscopy (see Immunohistochemistry and Imaging). The images were then analyzed using ImageJ.[60]

EV and IV collection and analysis

EVs were collected from conditioned media from COs and 2D cultured cells.[27] EVs collected from NPCs, d15 and d40 COs (unpatterned, dorsal and ventral) were obtained from two different IPSC lines, namely line C1[53] and line C3.[54] Only line C1 was used for all the other time points, for each developmental timepoint, EVs were collected from 4 independent differentiations (batches, biological replicates). For cells in 2D, EVs were pooled from at least 3 independent differentiations (biological replicates). We performed EV collection by the following steps: centrifugation at 300*g* for 10 min, supernatant centrifugation at 2000*g* for 10 min at 4°C, supernatant centrifugation at 10.000*g* for 30 min at 4°C, supernatant centrifugation at 100.000*g* for 90 min at 4°C in a fixed-angle rotor (TH865,

Thermo Fisher Scientific), followed by pellet wash with 1x PBS and centrifugation at 100.000*g* for 90 min at 4°C. Alternatively, miRCURY Exosome Cell/Urine/CSF Kit (Qiagen, 76743) was used to isolate EVs from conditioned medium according to the manufacturer instructions. For NPCs, EVs were collected from three independent cultures of control NPCs. Neuronal EVs were collected from three independent neuronal differentiation cultures at 8 to 10 weeks in cultures. Similarly, astrocyte EVs were collected from three independent cultures of astrocytes. For COs, EVs were collected from conditioned media of 20–30 different COs in culture.

IVs were isolated by subcellular fractionation. Briefly, a pool of 5–7 COs was homogenized and upon removal of nuclei, cell debris and mitochondrial fraction as previously reported,[61] the supernatatant was ultracentrifuged at 100.000 g for 30 min to obtain the cellular fraction (IVs).

For the nanoparticle tracking analysis (NTA), fresh, unfrozen extracellular vesicle suspensions were diluted in PBS and analyzed using a Particle Metrix ZetaView PMX110-Z Nanoparticle Tracking Analyzer (Particle Metrix GmbH, Inning am Ammersee, Germany) equipped with a 520 nm laser. For each measurement, samples were introduced manually, the temperature was set to 24°C, and two cycles were performed by scanning at 11 discrete positions in the cell channel and capturing 60 frames per position (video setting: high). The following recommended parameters were used for the measurement.

Sensitivity:	80.0
Shutter:	70
Frame rate:	30
Minimum Brightness:	20
Minimum Area:	5
Maximum Area:	1000
Maximum Brightness:	255
Tracking Radius2:	100
Minimum Tracelength:	15
nm/class:	5
Classes/decade:	64

After capture, the videos were analyzed for particle size and concentration using the ZetaView Software 8.05.12 SP1.

For immune-electron microscopy, aliquots of extracellular vesicle suspensions were anayzed by Dr Ilkka Miinalainen at Biocenter Oulu/EM laboratory, Finland.[62] Vesicles were deposited on Formvar carbon coated, glow-discharged grids and incubated in a blocking serum containing 1% BSA in PBS. CD81 and LGALS3 primary antibodies and secondary gold conjugates (Zymed, San Francisco, CA, USA) were diluted in 1% BSA in PBS. The blocking efficiency was controlled by performing the labeling procedure in the absence of primary antibody.

EV uptake assay in 2D cell cultures

NPCs, astrocytes and neurons were cultured in 24-well plates (see NPC, neuron and astrocyte cultures). 10–12 mL of conditioned media from at least 3 independent differentiations (biological replicates) were used for EV collection via ultracentrifugation. To fluorescently label the EVs, the conditioned media was treated with 1 μL of 10 mM DiI (1,1′-Dioctadecyl-3,3,3′,3′-Tetramethylindocarbocyanine Perchlorate) for 15 min in the dark before the final washing step in ultracentrifugation. The media of the recipient cells was changed just prior to the addition of the labeled EVs. EVs were then added to three individual coverslips with receiving cells. The cells were fixed 18 h after EV treatment with 4% paraformaldehyde for 15 min at room temperature.

EV uptake assay in sectioned COs

COs (d40) were rinsed in PBS and embedded in low-melting point agarose (Biozym Scientific GmbH, 850080). Embedded organoids were then cut into 250 μm thick sections using a VT1200s vibratome (Leica, Germany), approximately 3–4 sections were obtained per organoid, and 3 organoids were used per condition, Sections were then placed on Falcon Cell Culture Insert with a 0.4 μm pore PET membrane (Falcon, 353090) within a 6-well-plate. After 3 days in culture, fluorescently labeled EVs were added in a drop-wise manner on top of the CO sections and incubated for 18 h. Sections were then prepared for immunohistochemistry (see Immunohistochemistry).

Immunohistochemistry

Monolayer cultures of NPCs, neurons, and astrocytes were fixed with 4% paraformaldehyde for 15 min at room temperature, followed by three times 5 min washing with 1xPBS. Next, cells were blocked against unspecific binding and permeabilized in blocking buffer (10% normal goat serum, 0,02% Triton X- in 1xPBS) for 1 h. Primary antibodies diluted in blocking buffer were then added to the cells in the dilutions specified below (Key resources table) and incubated overnight. On the second day, cells were washed five times for 5 min each in PBS with 0,1% Tween (PBS-T), and then incubated at room temperature for 2 h in secondary antibodies raised

against the host animal of the primary antibody. Secondary antibodies were diluted in blocking buffer and the dilutions used are listed below (Key resources table). DAPI (4′,6-diamidino-2-phenylindole) was added as a nuclear counterstaining. Finally, cells were washed three times with PBS-T and mounted on object slides with Fluoromount-G (ThermoFisher Scientific, 00-4958-02). To validate the specificity of the primary antibodies, experiments were always performed with a secondary antibody-only sample as background control.

15-day-old COs were collected, rinsed in PBS and fixed in 4% paraformaldehyde for 30 min at room temperature. They were then placed in 30% sucrose solution for cryoprotection overnight at 4°C and frozen in O.C.T embedding compound for cryosectioning. 14 μm sections were collected in adhesion slides Superfrost Plus (Carl Roth, Germany) and stored at −20°C. For immunohistochemistry, slides were placed at room temperature for 45 min, rinsed in PBS and then incubated in blocking buffer (10% normal goat serum, 0,02% Triton X- in 1xPBS) for 1 h. Primary antibodies diluted in blocking buffer were then added to the slides in the dilutions specified below (Key resources table) and incubated overnight. The following day, slides were washed three times for 5 min each in PBS, and then incubated at room temperature for 2 h in secondary antibodies raised against the host animal of the primary antibody. Secondary antibodies were diluted in blocking buffer and the dilutions used are listed below (Key resources table). DAPI (4′,6-diamidino-2-phenylindole) was added as a nuclear counterstaining. Finally, the slides were washed three times with PBS and a coverslip was mounted with Fluoromount-G (ThermoFisher Scientific, 00-4958-02).

Imaging

Immunostainings were imaged with confocal microscopy or Stimulated Emission Depletion (STED) microscopy.

Confocal stack images were obtained using a Leica SP8 confocal microscope based on a DMi8 stand (Leica Microsystems, Wetzlar, Germany), equipped with 20x/0.75 (oil), 40x/1.10 (water), and 63x/1.30 (glyc) objectives. Images were then processed using ImageJ.[60]

STED imaging was performed with a TCS SP8 STED 3X FALCON confocal head (Leica Microsystems, Germany) mounted on an inverted microscope (DMi8; Leica Microsystems, Germany). For imaging, a 405 nm diode and a white light laser were used as excitation sources for DAPI, Alexa Flour 594 (ThermoFisher, USA), and ATTO 647N (ATTO-TEC GmbH, Germany) (405 nm, 575 nm, 644 nm lasers lines respectively). Single photons were collected through a 100×/1.4 NA oil-immersion objective and detected on Hybrid Detectors (HyD) (Leica Microsystems) with a 420–500 nm, 590–670 nm, 660–720 nm spectral detection window for DAPI, Alexa Flour 594, and ATTO 647N detection, respectively. For depletion, a 775 nm pulsed laser was used for Alexa Fluor 594 and ATTO 647N. DAPI was not depleted and only imaged with confocal resolution. The image size was set to 1024 × 1024 pixels and a 5-fold zoom factor was applied, giving a pixel size of 0.023 μm and an image size of 23,25 × 23,25 μm. For FLIM, the white light laser delivered 80 MHz repetition rate. Arrival time of single photons was measured with the included FALCON module and 8 frames were acquired at a scanning speed of 200 Hz. Recordings were done sequentially for each dye to avoid crosstalk. Raw STED images were further processed with the τ-STED module of LAS X software (Leica Microsystems, Germany) increasing further the resolution thanks to the lifetime information recorded.

For the live imaging of EV uptake by NPCs, NPCs were seeded in a 24-well-plate at a density of 15,000 cells/well. 48h after seeding, 6 wells of cells were treated with NucSpot 488 Live Cell Nuclear Stain as suggested by the supplier (Biotium, U.S.A). Of the 6 wells, 3 wells were then treated with DiI-labelled EVs collected from 12 mL of media, while 3 wells were treated with diluted DiI as a negative control. The cells were imaged for 24h using a Leica TIRF system and a 100x/1.47 NA objective. The videos obtained were analyzed using ImageJ.[60]

3D image reconstruction was conducted using Imaris v9.7.2 (Oxford Instruments). The fluorescence signal of confocal z-stacks with intervals of 250 nm was represented by surface visualization using the default threshold parameters recommended by the software. Snapshots of the 3D rendered images were then captured.

Microfluidics chamber

A silicone device with a 900 μm microgroove barrier (ref. SND900, Xona Microfluidics, USA) was used to co-culture an RFP-labelled NPC cell line and non-fluorescently labeled neurons in independent chambers. Each cell line was maintained in their corresponding media (see NPC, neuron and astrocyte cultures) and after 7 days of being co-cultured, the cells were fixed, immunostained and imaged using confocal microscopy (see Immunohistochemistry and Imaging).

Proteomic analysis

Sample preparation for mass spectrometry

Purified EVs, collected from the conditioned media of 20–30 COs in culture, and IVs, isolated from a pool of 5–7 COs, were lysed in RIPA buffer (150mM NaCl, 50mM Tris pH8, 0.1% DOC, 0.1% SDS, 0.1% NP40). 10 μg of protein for each sample was subjected to the modified FASP protocol.[63] Briefly, the protein extract was loaded onto the centrifugal filter CO10 kDa (Merck Millipore, Darmstadt, Germany), and detergent were removed by washing five times with 8M Urea (Merck, Darmstadt, Germany) 50mM Tris (Sigma-Aldrich, USA) buffer. Proteins were reduced by adding 5mM dithiothreitol (DTT) (Bio-Rad, Canada) at 37°C for 1 h in the dark. To remove the excess of DTT, the protein sample was washed three times with 8M Urea, 50mM Tris. Subsequently protein thiol groups were blocked with 10mM iodoacetamide (Sigma-Aldrich, USA) at RT for 45 min. Before proceeding with the enzymatic digestion, urea was removed by washing the protein suspension three times with 50mM ammonium bicarbonate (Sigma-Aldrich, Spain).

Proteins were digested first by Lys-C (Promega, USA) at RT for 2 h, then by trypsin (Premium Grade, MS Approved, SERVA, Heidelberg, Germany) at RT, overnight, both enzymes were added at an enzyme-protein ratio of 1:50 (w/w). Peptides were recovered by centrifugation followed by two additional washes with 50mM ammonium bicarbonate and 0.5M NaCl (Sigma-Aldrich, Switzerland). The two filtrates were combined, the recovered peptides were lyophilized under vacuum. Dried tryptic peptides were desalted using C18-tips (Thermo Scientific, Pierce, USA), following the manufacture instructions. Briefly, the peptides dissolved in 0.1%(v/v) formic acid (Thermo scientific, USA) were loaded onto the C18-tip and washed 10 times with 0.1% (v/v) formic acid, subsequently the peptides were eluted by 95% (v/v) acetonitrile (Merck, Darmstadt, Germany), 0.1% (v/v) formic acid. The desalted peptides were lyophilized under vacuum. The purified peptides were reconstituted in 0.1% (v/v) formic acid for LC-MS/MS analysis.

MS data acquisition

Desalted peptides were loaded onto a 25 cm, 75 μm ID C18 column with integrated nanospray emitter (Odyssey/Aurora, ionopticks, Melbourne) via the autosampler of the Thermo Easy-nLC 1000 (Thermo Fisher Scientific) at 60°C. Eluting peptides were directly sprayed onto the timsTOF Pro (Bruker Daltonics). Peptides were loaded in buffer A (0.1% (v/v) formic acid) at 400 nL/min and percentage of buffer B (80% acetonitril, 0.1% formic acid) was ramped from 5% to 25% over 90 min followed by a ramp to 35% over 30 min then 58% over the next 5 min, 95% over the next 5 min and maintained at 95% for another 5 min. Data acquisition on the timsTOF Pro was performed using timsControl. The mass spectrometer was operated in data-dependent PASEF mode with one survey TIMS-MS and ten PASEF MS/MS scans per acquisition cycle. Analysis was performed in a mass scan range from 100 to 1700 m/z and an ion mobility range from 1/K0 = 0.85 Vs. cm-2 to 1.30 Vs. cm-2 using equal ion accumulation and ramp time in the dual TIMS analyzer of 100 ms each at a spectra rate of 9.43 Hz. Suitable precursor ions for MS/MS analysis were isolated in a window of 2 Th for m/z < 700 and 3 Th for m/z > 700 by rapidly switching the quadrupole position in sync with the elution of precursors from the TIMS device. The collision energy was lowered as a function of ion mobility, starting from 45 eV for 1/K0 = 1.3 Vs. cm-2 to 27eV for 0.85 Vs. cm-2. Collision energies were interpolated linear between these two 1/K0 values and kept constant above or below these base points. Singly charged precursor ions were excluded with a polygon filter mask and further m/z and ion mobility information was used for 'dynamic exclusion' to avoid re-sequencing of precursors that reached a 'target value' of 14500 a.u. The ion mobility dimension was calibrated linearly using three ions from the Agilent ESI LC/MS tuning mix (m/z, 1/K0: 622.0289, 0.9848 Vs. cm-2; 922.0097 Vs. cm-2, 1.1895 Vs. cm-2; 1221.9906 Vs. cm-2, 1.3820 Vs. cm-2).

Raw data analysis of MS measurements

Raw data were processed using the MaxQuant computational platform (version 1.6.17.0)[64] with standard settings applied for ion mobility data.[65] Shortly, the peak list was searched against the Uniprot database of Human database (75069 entries, downloaded in July 2020) with an allowed precursor mass deviation of 10 ppm and an allowed fragment mass deviation of 20 ppm. MaxQuant by default enables individual peptide mass tolerances, which was used in the search. Cysteine carbamidomethylation was set as static modification, and methionine oxidation, deamidation and N-terminal acetylation as variable modifications. The match-between-run option was enabled, and proteins were quantified across samples using the label-free quantification algorithm in MaxQuant generating label-free quantification (LFQ) intensities.

Bioinformatic analysis

For the proteomic characterization in IVs and EVs, 7486 proteins were quantified. Proteins that were consistently detected in 2 of the 3 technical replicates per each condition were retained. Downstream analysis was performed using R. The LFQs values were log2-transformed. Missing values were imputed using the R package DEP (version 1.15.0) and replaced by random values of a left-shifted Gaussian distribution (shift of 1.8 units of the standard deviation and a width of 0.3). Differentially expression (DE) analysis was performed on the imputed data using Student's t Test. Proteins with log2 fold change values (log2FC) ≥ 1 and ≤ -1 and with an FDR-corrected q-value <0.05 were considered as differentially expressed (exodevo.psych.mpg.de/app/exodevo).[52]

Validation of proteomic results with automated western blot

EVs samples were collected from independent new cultures of COs and cells. 1 μg of proteins were loaded on automated western blot system (Proteinsimple WES, https://www.proteinsimple.com) with 12–230 kDa (SM-W004) or 66–440 kDa (SM-W006) Jess/Wess Separation Modules according to the molecular weight of the analyzed protein. All the antibodies were diluted 1:50 (Key resources table). Figures S1F, S2J, and S3A show the protein simple profiles and relative quantifications performed using ImageJ Software.

Single-cell RNA-sequencing

Single-cell dissociation was performed on five 60 days old-patterned spheroids randomly selected for each pattern condition. Single cells were dissociated using StemPro Accutase Cell Dissociation Reagent (Life Technologies), filtered through 30 μM and 20 μM filters (Miltenyi Biotec) and cleaned of debris using a Percoll (Sigma, P1644) gradient. Single cells were resuspended in ice-cold Phosphate-Buffered Saline (PBS) supplemented with 0.04% Bovine Serum Albumin at a concentration of 1000 cells per ul. Single cells were loaded onto a Chromium Next GEM Single Cell 3' chip (Chromium Next GEM Chip G Single Cell Kit, 16 rxns 10XGenomics PN-1000127) with the Chromium Next GEM Single Cell 3' GEM, Library & Gel Bead Kit v3.1 (Chromium Next GEM Single Cell 3' GEM, Library & Gel Bead Kit v3.1, 4 rxns 10xGenomics PN-1000128) and cDNA libraries were generated with the Single Index Kit T Set A, 96 rxns (10xGenomics PN-1000213) according to the manufacturer's instructions. Libraries were sequenced using Illumina NovaSeq6000 in 28/8/91bp mode (SP flowcell), quality control and UMI counting were performed by the Max-Planck für molekulare

Genetik (Germany). Downstream analysis was performed using the R package Seurat (version 3.2). Cells with more than 2,500 or less than 200 detected genes or with mitochondrial content higher that 10% were excluded as well as genes that were not expressed in at least three cells. Normalization of gene expression was done using a global-scaling normalization method (“LogNormalize”, scale.factor = 10000) and the 2000 most variable genes were selected (selection method, “vst”) and scaled (mean = 0 and variance = 1 for each gene) before principal component analysis. The “FindNeighbors” and “FindClusters” functions were used for clustering with resolution of 0.5 and UMAP for visualization. Clusters were grouped based of the expression of known marker genes and differentially expressed gene identified with the “FindAllMarkers” function.

Bulk-RNA-sequencing

RNA-seq was performed on 10ng of total RNA collected from 3 independent wells of NPCs from a 24well plate. NPCs were not treated with EVS or treated for 12h with EVs collected by ultracentrifugation from 25 mL of conditioned medium collected from 28 to 37 days in culture COs (control ventral, EPM1 ventral, control dorsal and EPM1 dorsal COs). NPCs were lysed in 1mL Trizol (Qiagen)/well and RNA was isolated employing RNA Clean & Concentrator kit (Zymo Research) including digestion of remaining genomic DNA according to producer’s guidelines. RNA was further processed according to.[66] Briefly, cDNA synthesis was performed with SMART-Seq v4 Ultra Low Input RNA Kit (Clontech cat. 634888) according to the manufacturer’s instruction. cDNA was fragmented to an average size of 200–500 bp in a Covaris S220 device (5 min; 4°C; PP 175; DF 10; CB 200). Fragmented cDNA was used as input for library preparation with MicroPlex Library Preparation Kit v2 (Diagenode, cat. C05010012) and processed according to the manufacturer’s instruction. Libraries were quality controlled by Qubit and Agilent DNA Bioanalyzer analysis. Deep sequencing was performed on a HiSeq 1500 system according to the standard Illumina protocol for 50 bp paired-end reads with v3 sequencing reagents.

RNAseq analysis

Paired end reads were aligned to the human genome version GRCh38 using STAR v2.6.1d[67] with default options "–runThreadN 32 –quantMode TranscriptomeSAM GeneCounts –outSAMtype BAM SortedByCoordinate". Reads-per-gene counts were imported in R v4.1.0. Bioconductor package DESeq2 v1.32.0[68] was used for differential expression analysis. Only genes with read counts>1 were considered. Significantly changed genes were determined through pairwise comparisons using the DESeq2 results function (log2 fold change threshold = 1, adjusted p-value <0.05). Heatmaps with differentially expressed genes were plotted with pheatmap v1.0.12 and RColorBrewer v1.1-2 using rlog-normalized expression values.

QUANTIFICATION AND STATISTICAL ANALYSIS

Quantification of EV markers in cell types

The expression of standard EV markers (CD63, CD81, CD82, CD9 and PDCD6IP) was quantified via immunohistochemistry in monolayer cultures of NPCs, young neurons, mature neurons and astrocytes. Immunohistochemistry was conducted as mentioned above using the antibodies and dilutions stated in Key resources table. Immunoreactivity was quantified using ImageJ.[60] A cell was counted as positive for an EV marker if immunoreactivity was observed within the nucleus or in the cytoplasm of the cell. Since neurons generate long projections which are difficult to image to their full extent, only the somas and proximal neurites were quantified as being positive for each EV marker. In NPCs and astrocytes, a cell was counted as positive for an EV marker if immunoreactivity was detected in the nucleus or in the cytoplasm in close proximity to the nucleus since they are cultured in high confluency and therefore sometimes complicating the discrimination between cells. All the statistical details of this quantification can be found in the figure legend.

Quantification of EV uptake by cell types

The uptake of pEVs, nEVs and aEVs by NPCs, neurons (young and mature) and astrocytes was quantified in three individual coverslips of receiving cells by counting the number of cells which had DiI-positive EVs (see EV uptake assay) in either the nucleus or cytoplasm using ImageJ.[60] Since neurons generate long projections which are difficult to image to their full extent, only the somas and proximal neurites were quantified. In NPCs and astrocytes, a cell was counted as positive for an EV marker if immunoreactivity was detected in the nucleus or in the cytoplasm in close proximity to the nucleus since they are cultured in high confluency and therefore sometimes complicating the discrimination between cells.

The number of particles was also quantified in receiving cells using the option “Analyze particles” available in ImageJ.[60] First, a mask was generated from an image with a cytoplasmic marker to outline the cells. Then, EV images were converted to binary with an automatic threshold, and particles ranging from 100 to 300 nm within the cell outline mask were counted with no filtering done for circularity. All the statistical details of these quantifications can be found in the figure legend.

Quantification of EV uptake by CO sections

Images of EV-treated CO sections were analyzed using ImageJ.[60] First, masks were generated for the progenitor zone using Nestin as a marker, and for the cortical plate using DCX as a marker. Then, the number of particles were counted using the “Analyze

particles'' option within these delimited areas using the masks previously generated. EV images were converted to binary with an automatic threshold, and particles ranging from 100 to 300 nm with no filtering done for circularity. All the statistical details of this quantification can be found in the figure legend.

Proteomic statistical analysis

Missing values were imputed using the R package DEP (version 1.15.0) and replaced by random values of a left-shifted Gaussian distribution (shift of 1.8 units of the standard deviation and a width of 0.3). Differentially expression (DE) analysis was performed on the imputed data using Student's t Test. Proteins with log2 fold change values (log2FC) ≥ 1 and ≤ -1 and with an FDR-corrected q-value <0.05 were considered as differentially expressed (exodevo.psych.mpg.de/app/exodevo).

RNAseq statistical analysis

Bioconductor package DESeq2 v1.32.0[68] was used for differential expression analysis. Only genes with read counts>1 were considered. Significantly changed genes were determined through pairwise comparisons using the DESeq2 results function (log2 fold change threshold = 1, adjusted *p*-value <0.05). Heatmaps with differentially expressed genes were plotted with pheatmap v1.0.12 and RColorBrewer v1.1-2 using rlog-normalized expression values.

Enrichment analysis

GO term analysis of differentially expressed proteins was tested using the FUMA algorithm[69] by inserting the DE protein lists into the GENE2FUNC software (FDR<0.05) (https://fuma.ctglab.nl/) or with STRING (https://string-db.org).